REPORT DOCUMENTATION PAGE

Form Approved OMB NO. 0704-0188

1. REPORT DATE (DD-MM-YYYY)	2. REPORT TYPE	3. DATES COVERED (From - To)
29-12-2015	Final Report	1-Oct-2012 - 30-Sep-2015

4. TITLE AND SUBTITLE
Final Report: Novel Optical Fiber Materials With Engineered Brillouin Gain Coefficients SSL-1: NOVEL FIBER LASERS

5a. CONTRACT NUMBER
W911NF-12-1-0602

5b. GRANT NUMBER

5c. PROGRAM ELEMENT NUMBER

6. AUTHORS
Peter Dragic, John Ballato

5d. PROJECT NUMBER

5e. TASK NUMBER

5f. WORK UNIT NUMBER

7. PERFORMING ORGANIZATION NAMES AND ADDRESSES
University of Illinois - Urbana
1901 S. First Street, Suite A
Champaign, IL 61820 -7406

8. PERFORMING ORGANIZATION REPORT NUMBER

9. SPONSORING/MONITORING AGENCY NAME(S) AND ADDRESS (ES)
U.S. Army Research Office
P.O. Box 12211
Research Triangle Park, NC 27709-2211

10. SPONSOR/MONITOR'S ACRONYM(S)
ARO

11. SPONSOR/MONITOR'S REPORT NUMBER(S)
62081-PH-HEL.25

12. DISTRIBUTION AVAILIBILITY STATEMENT
Approved for Public Release; Distribution Unlimited

13. SUPPLEMENTARY NOTES
The views, opinions and/or findings contained in this report are those of the author(s) and should not contrued as an official Department of the Army position, policy or decision, unless so designated by other documentation.

14. ABSTRACT
This 2-year program (with 1 year no-cost extension) sought to investigate novel optical materials suitable for use in high-power narrow-linewidth fiber lasers. A complete model for the mass density, acoustic velocity, acoustic attenuation, photoelastic (Pockels') coefficients, and refractive index has been developed for multi-component glasses. It has been utilized to characterize several materials (data are provided herein), including Group I and II oxides, MgAl2O4 (spinel), alumina, LuAG (a garnet), and several rare earths (RE2O3), including determination of compositions that give rise to near-zero Brillouin gain. Fibers were produced from these precursors (crystal and

15. SUBJECT TERMS
High energy lasers, optical fiber, glass design, molten core fabrication, Pockels coefficients, acoustic properties, Brillouin scattering, Raman scattering, nonlinear fiber optics, novel materials

16. SECURITY CLASSIFICATION OF:			17. LIMITATION OF ABSTRACT	15. NUMBER OF PAGES	19a. NAME OF RESPONSIBLE PERSON
a. REPORT	b. ABSTRACT	c. THIS PAGE			Peter Dragic
UU	UU	UU	UU		19b. TELEPHONE NUMBER 217-333-8399

Report Title

Final Report: Novel Optical Fiber Materials With Engineered Brillouin Gain Coefficients SSL-1: NOVEL FIBER LASERS

ABSTRACT

This 2-year program (with 1 year no-cost extension) sought to investigate novel optical materials suitable for use in high-power narrow-linewidth fiber lasers. A complete model for the mass density, acoustic velocity, acoustic attenuation, photoelastic (Pockels') coefficients, and refractive index has been developed for multi-component glasses. It has been utilized to characterize several materials (data are provided herein), including Group I and II oxides, MgAl2O4 (spinel), alumina, LuAG (a garnet), and several rare earths (RE2O3), including determination of compositions that give rise to near-zero Brillouin gain. Fibers were produced from these precursors (crystal and glass phase), clad in silica, utilizing the molten core processing technique. Measurement test beds have been developed to determine the key acoustic and photoelastic constants of these fibers, in order to validate the model. Within the scope of this work, suppression of Brillouin scattering by >10dB relative to conventional fiber has been 'routine.' Furthermore, we have investigated some rare-earth-doped versions of these fibers, and other novel materials have been identified as promising and these were continued to be studied during the extension period. We point out that this limited report represents only highlights from the numerous findings accumulated during this program. They can be found in greater detail in the roughly 175 printed pages in the resulting 17 journal publications (quite a bit more if one includes a number of archival conference proceedings).

Enter List of papers submitted or published that acknowledge ARO support from the start of the project to the date of this printing. List the papers, including journal references, in the following categories:

(a) Papers published in peer-reviewed journals (N/A for none)

Received		Paper
04/02/2013	1.00	Anthony Mangognia, Courtney Kucera, Jonathon Guerrier, Joshua Furtick, Thomas Hawkins, Peter D. Dragic, John Ballato. Spinel-derived single mode optical fiber, Optical Materials Express, (03 2013): 511. doi: 10.1364/OME.3.000511
05/07/2013	2.00	P. Dragic, C. Kucera, J. Furtick, J. Guerrier, T. Hawkins, J. Ballato. Brillouin spectroscopy of a novel baria-doped silica glass optical fiber, Optics Express, (04 2013): 0. doi: 10.1364/OE.21.010924
07/29/2013	4.00	Peter D. Dragic, John Ballato, Stephanie Morris, Thomas Hawkins. The Brillouin gain coefficient of Yb-doped aluminosilicate glass optical fibers, Optical Materials, (07 2013): 0. doi: 10.1016/j.optmat.2013.04.006
07/29/2013	3.00	J. Ballato, P.D. Dragic. Characterisation of Raman gain spectra in Yb:YAG-derived optical fibres, Electronics Letters, (07 2013): 0. doi: 10.1049/el.2013.1386
08/28/2014	7.00	John Ballato, Peter D. Dragic. 120 Years of Optical Glass Science, Optics and Photonics News, (05 2014): 0. doi: 10.1364/OPN.25.5.000044
08/28/2014	8.00	John Ballato, Peter Dragic. Materials Development for Next Generation Optical Fiber, Materials, (06 2014): 0. doi: 10.3390/ma7064411
08/28/2014	11.00	P. D. Dragic, C. Kucera, J. Ballato, D. Litzkendorf, J. Dellith, K. Schuster. Brillouin scattering properties of lanthano–aluminosilicate optical fiber, Applied Optics, (08 2014): 0. doi: 10.1364/AO.53.005660
12/28/2015	16.00	Colin Ryan, Peter Dragic, Joshua Furtick, Courtney J. Kucera, Roger Stolen, John Ballato. Pockels Coefficients in Multicomponent Oxide Glasses, International Journal of Applied Glass Science, (12 2015): 0. doi: 10.1111/ijag.12146
12/28/2015	17.00	Peter D. Dragic, Steve W. Martin, Arthur Ballato, John Ballato. On the Anomalously Strong Dependence of the Acoustic Velocity of Alumina on Temperature in Aluminosilicate Glass Optical Fibers-Part I: Material Modeling and Experimental Validation, International Journal of Applied Glass Science, (08 2015): 0. doi: 10.1111/ijag.12137
12/28/2015	13.00	Peter D. Dragic, Anthony Mangognia, John Ballato. Chirped fiber Brillouin frequency-domain distributed sensing, Optical Engineering, (05 2014): 0. doi: 10.1117/1.OE.53.5.056117
12/28/2015	14.00	Stephen J. Mihailov, John Ballato, Peter D. Dragic, Dan Grobnic. Type I and II Bragg gratings made with infrared femtosecond radiation in high and low alumina content aluminosilicate optical fibers, Optica, (03 2015): 0. doi: 10.1364/OPTICA.2.000313
12/28/2015	18.00	Steve W. Martin, John Ballato, Arthur Ballato, Peter D. Dragic. On the Anomalously Strong Dependence of the Acoustic Velocity of Alumina on Temperature in Aluminosilicate Glass Optical Fibers-Part II: Acoustic Properties of Alumina and Silica Polymorphs, and Approximations of the Glassy State, International Journal of Applied Glass Science, (08 2015): 0. doi: 10.1111/ijag.12141

12/28/2015	19.00	P. D. Dragic, C. J. Kucera, M. Cavillon, M. Tuggle, M. Jones, T. W. Hawkins, C. Ryan, A. D. Yablon, R. Stolen, J. Ballato. Single- and few-moded lithium aluminosilicate optical fiber for athermal Brillouin strain sensing, Optics Letters, (10 2015): 0. doi: 10.1364/OL.40.005030

TOTAL: **13**

Number of Papers published in peer-reviewed journals:

(b) Papers published in non-peer-reviewed journals (N/A for none)

Received		Paper
08/29/2013	6.00	John Ballato, Peter Dragic. Rethinking Optical Fiber: New Demands, Old Glasses, Journal of the American Ceramic Society, (04 2013): 0. doi:

TOTAL: **1**

Number of Papers published in non peer-reviewed journals:

(c) Presentations

[7] Invited Paper. J. Ballato, T. Hawkins, and P. Dragic, to be presented at ICC 2014.

[6] Invited Paper. J. Ballato, T. Hawkins, and P. Dragic, "Novel Rare-earth Doped Optical Fibers with Intrinsically Low Brillouin and Raman Gain," presented at the 5th International Workshop on Photoluminescence in Rare Earths: Photonic Materials and Devices (PRE ' 14), May 13 – 16, 2014, San Sebastian, Spain.

[5] J. Ballato and P. Dragic, "Brillouin-almost-free optical fibers," presented at the Fiber Society Fall Symposium, Clemson, SC, October 25, 2013.

[4] J. Ballato, P.D. Dragic, and T. Hawkins, "Intrinsically low Brillouin- and Raman-scattering optical fibers," Proc. SPIE, paper 8961-42.

[3] Invited Paper. J. Ballato and P. Dragic, "Novel Brillouin-Suppressing Optical Fibers," presented at the Advanced Solid State Lasers (ASSL) OSA Congress, Paris, France, October 27 – November 1, 2013.

[2] J. Ballato, "Molten Core Fabrication of Novel Optical Fibers," Advanced Fibre Photonics Technologies workshop, Le Centre National de la Recherche Scientifique, Institute for Engineering and Systems Sciences (INSIS), Paris, France, October 2013.

[1] J. Ballato and P. Dragic, "Molten Core Fabrication of Novel Optical Fibers," Innovations in Glass Science and Technology - 2013 Glass and Optical Materials Division (GOMD) Meeting, Glasses for Optoelectronic and Optical Applications Symposium, 10th Pacific Rim Conference on Ceramic and Glass Technology, San Diego, CA, June 2013.

Number of Presentations: 7.00

Non Peer-Reviewed Conference Proceeding publications (other than abstracts):

Received		Paper
07/29/2013	5.00	Peter D. Dragic, John Ballato, Stephanie Morris, Thomas Hawkins. Intrinsically-low Brillouin gain optical fibers, SPIE Defense, Security, and Sensing. 23-MAY-13, Baltimore, Maryland, USA. : ,
08/28/2014	9.00	Peter Dragic, John Ballato, Thomas Hawkins. Compositional tuning of glass for the suppression of nonlinear andparasitic fiber laser phenomena, Laser Technology for Defense and Security X. 04-MAY-14, . : ,
TOTAL:	**2**	

Number of Non Peer-Reviewed Conference Proceeding publications (other than abstracts):

Peer-Reviewed Conference Proceeding publications (other than abstracts):

Received		Paper
08/28/2014	10.00	Peter D. Dragic. Intrinsically Low Brillouin Gain Fibers (How Low Can You Go?), Frontiers in Optics. , Orlando, Florida. : ,
08/28/2014	12.00	John Ballato. Rethinking Optical Fiber: New Demands, Old Glasses, Workshop on Specialty Optical Fibers and their Applications. , Sigtuna. : ,
12/28/2015	24.00	J. Ballato, P. Dragic. Novel Brillouin- and Raman-suppressing optical fibers, 2014 IEEE Photonics Conference (IPC). 11-OCT-14, San Diego, CA. : ,
12/28/2015	22.00	Peter D. Dragic, John Ballato, Stephanie Morris, Alex Evert, Robert R. Rice, Thomas Hawkins. Novel optical fibers for Brillouin-based distributed sensing, SPIE Defense, Security, and Sensing. 29-APR-13, Baltimore, Maryland, USA. : ,
12/28/2015	23.00	Dan Grobnic, Stephen J. Mihailov, John Ballato, Peter Dragic. Bragg Gratings Made with IR Femtosecond Radiation in High Alumina Content Aluminosilicate Optical Fibers, Bragg Gratings, Photosensitivity, and Poling in Glass Waveguides. 27-JUL-14, Barcelona. : ,
TOTAL:	**5**	

Number of Peer-Reviewed Conference Proceeding publications (other than abstracts):

(d) Manuscripts

Received	Paper
12/28/2015 15.00	John Ballato, Peter Dragic. Towards the Perfect Optical Fiber, Journal of the South Carolina Academy of Science (12 2014)
12/28/2015 20.00	Colin Ryan, Matthew Tuggle, Maxwell Jones, Thomas Wade Hawkins, Peter Dragic, John Ballato, Courtney J. Kucera, Maxime Cavillon, Joshua Furtick. Brillouin Properties of a Novel StrontiumAluminosilicate Glass Optical Fiber, Journal of Lightwave Technology (10 2015)
12/28/2015 21.00	P D Dragic, M G Pamato, V Iordache, J D Bass, C J Kucera, M Jones, T W Hawkins, J Ballato. Athermal distributed Brillouin sensors utilizing all-glass optical fibersfabricated from rare earth garnets: LuAG, New Journal of Physics (09 2015)
TOTAL:	**3**

Number of Manuscripts:

Books

Received	Book
TOTAL:	

Received	Book Chapter
TOTAL:	

Patents Submitted

Invention disclosures are still being processed by the IP departments at Clemson and Illinois.

Patents Awarded

Awards

5 invited presentations
5 invited journal papers
1 journal cover
1 paper awarded "Spotlight on Optics" by the Optical Society of America
1 paper awarded Author Interview

Graduate Students

NAME	PERCENT_SUPPORTED	Discipline
Anthony Mangognia	0.80	
Colin Ryan	1.00	
Maxime Cavillon	1.00	
Laura Burka	1.00	
Stephanie Morris	0.50	
FTE Equivalent:	**4.30**	
Total Number:	**5**	

Names of Post Doctorates

NAME	PERCENT_SUPPORTED
FTE Equivalent:	
Total Number:	

Names of Faculty Supported

NAME	PERCENT_SUPPORTED	National Academy Member
Peter Dragic	0.13	
John Ballato	0.05	
FTE Equivalent:	**0.18**	
Total Number:	**2**	

Names of Under Graduate students supported

NAME	PERCENT_SUPPORTED	Discipline
Riccardo Fabbro	1.00	Electrical Engineering
John Andrew Krol	1.00	Electrical Engineering
Maxime Cavillon	1.00	Materials Science
Matthew Tuggle	1.00	Materials Science
FTE Equivalent:	**4.00**	
Total Number:	**4**	

Student Metrics

This section only applies to graduating undergraduates supported by this agreement in this reporting period

The number of undergraduates funded by this agreement who graduated during this period:	3.00
The number of undergraduates funded by this agreement who graduated during this period with a degree in science, mathematics, engineering, or technology fields:	3.00
The number of undergraduates funded by your agreement who graduated during this period and will continue to pursue a graduate or Ph.D. degree in science, mathematics, engineering, or technology fields:	2.00
Number of graduating undergraduates who achieved a 3.5 GPA to 4.0 (4.0 max scale):	3.00
Number of graduating undergraduates funded by a DoD funded Center of Excellence grant for Education, Research and Engineering:	0.00
The number of undergraduates funded by your agreement who graduated during this period and intend to work for the Department of Defense	0.00
The number of undergraduates funded by your agreement who graduated during this period and will receive scholarships or fellowships for further studies in science, mathematics, engineering or technology fields:	0.00

Names of Personnel receiving masters degrees

NAME
Laura Burka
Total Number: **1**

Names of personnel receiving PHDs

NAME
Anthony Mangognia
Stephanie Morris
Total Number: **2**

Names of other research staff

NAME	PERCENT_SUPPORTED
Courtney Kucera	0.21
Maxwell Jones	0.50
FTE Equivalent:	**0.71**
Total Number:	**2**

Sub Contractors (DD882)

1 a. Clemson University

1 b. Office of Sponsored Programs

Clemson SC 29634

Sub Contractor Numbers (c):

Patent Clause Number (d-1):

Patent Date (d-2):

Work Description (e):

Sub Contract Award Date (f-1):

Sub Contract Est Completion Date(f-2):

Inventions (DD882)

5 **Brillouin athermal optical fibers**

Patent Filed in US? (5d-1) N

Patent Filed in Foreign Countries? (5d-2) N

Was the assignment forwarded to the contracting officer? (5e) N

Foreign Countries of application (5g-2): none yet

5a: John Ballato

5f-1a: Clemson University

5f-c:

5a: Peter Dragic

5f-1a: University of Illinois at Urbana-Champaign

5f-c:

5 **Suppression of Stimulated Raman Scattering (SRS) in Optical Fibers**

Patent Filed in US? (5d-1) N

Patent Filed in Foreign Countries? (5d-2) N

Was the assignment forwarded to the contracting officer? (5e) Y

Foreign Countries of application (5g-2): none

5a: John Ballato

5f-1a: Clemson University

5f-c:

5a: Peter Dragic

5f-1a: University of Illinois at Urbana-Champaign

5f-c:

Scientific Progress

This 2-year program (with 1 year no-cost extension) sought to investigate novel optical materials suitable for use in high-power narrow-linewidth fiber lasers. A complete model for the mass density, acoustic velocity, acoustic attenuation, photoelastic (Pockels') coefficients, and refractive index has been developed for multi-component glasses. It has been utilized to characterize several materials (data are provided herein), including Group I and II oxides, MgAl2O4 (spinel), alumina, LuAG (a garnet), and several rare earths (RE2O3), including determination of compositions that give rise to near-zero Brillouin gain. Fibers were produced from these precursors (crystal and glass phase), clad in silica, utilizing the molten core processing technique. Measurement test beds have been developed to determine the key acoustic and photoelastic constants of these fibers, in order to validate the model. Within the scope of this work, suppression of Brillouin scattering by >10dB relative to conventional fiber has been 'routine.' Furthermore, we have investigated some rare-earth-doped versions of these fibers, and other novel materials have been identified as promising and these were continued to be studied during the extension period.

Technology Transfer

none

Summary of Technical Achievements

Proposal Number 62081-PH-HEL

Agreement Number W911NF-12-1-0602

Final Report

Peter D. Dragic (PI)

John Ballato (Co-PI)

Statement of the Problem Studied

This 2-year program (with 1 year no-cost extension) sought to investigate novel optical materials suitable for use in high-power narrow-linewidth fiber lasers. A complete model for the mass density, acoustic velocity, acoustic attenuation, photoelastic (Pockels') coefficients, and refractive index has been developed for multi-component glasses. It has been utilized to characterize several materials (data are provided herein), including Group I and II oxides, $MgAl_2O_4$ (spinel), alumina, LuAG (a garnet), and several rare earths (RE_2O_3), including determination of compositions that give rise to near-zero Brillouin gain. Fibers were produced from these precursors (crystal and glass phase), clad in silica, utilizing the molten core processing technique. Measurement test beds have been developed to determine the key acoustic and photoelastic constants of these fibers, in order to validate the model. Within the scope of this work, suppression of Brillouin scattering by >10dB relative to conventional fiber has been 'routine.' Furthermore, we have investigated some rare-earth-doped versions of these fibers, and other novel materials have been identified as promising and these were continued to be studied during the extension period. We point out that this limited report represents only highlights from the numerous findings accumulated during this program. They can be found in greater detail in the roughly 175 printed pages in the resulting 17 journal publications (quite a bit more if one includes a number of archival conference proceedings). Sections II – V provide the Summary of the Most Important Results.

Table of Contents

List of Figures and Tables

Figure 4. Optical micrograph of spinel-derived (i) and BaO-derived (ii) fiber cross-sections, splices between silica and the (iii) spinel-derived and (iv) BaO-derived fibers. In (iii) and (iv), "SpDF" refers to the spinel-derived optical fiber and "BaODF" refers to the BaO-derived optical fiber.

Figure 5. Brillouin gain coefficient versus alumina concentration in mole % for several ytterbia concentrations, increasing from 0 to 1 mole % (~ 6 wt%) in steps of 0.1 mol %.

Figure 6. Brillouin gain coefficient versus P_2O_5 concentration in mole % for several ytterbia concentrations, increasing from 0 to 1 mole % (~ 6 wt%).

Figure 7. Overlay of the Yb-doped aluminosilicate emission spectrum (black) with that of a Yb-doped bariosilicate glass (blue). They are nearly indistinguishable.

Figure 8. RIPs measured at 1000 nm and 1550 nm (the latter has a slightly higher peak Δn). The data taken at 1000 nm is shown with the dashed line.

Figure 9. SEM image of the SAL fiber core. A slight ellipticity is observed.

Figure 10. Brillouin gain coefficient calculated for the lanthanum aluminosilicate system (bulk) utilizing the parameters in [30] and assuming that $[Al_2O_3] = 1.21x[La_2O_3]$.

Figure 11. Scanning electron microscope end image (fiber cross section) of Fibers 1 and 2 with scale provided. There is some ellipticity in the Fiber 2 core.

Figure 12. Attenuation spectrum for the fibers. Hydroxyl absorption near 1400 is observed. The remaining structure can be attributed to optical absorption bands of various other rare earth impurities present in the starting LuAG crystal.

Figure 13. Refractive index profiles for Fiber 1 (open circles) and Fiber 2 (solid squares).

Figure 14. Molar ratio of Lu to Al across the core of Fiber 2.

Figure 15. Calculated Brillouin coefficient (g_B) relative to a typical Ge-doped SMF versus a ratio of SiO_2-SrO-Al_2O_3 content for the ternary strontium aluminosilicate glasses. A zero-p_{12} composition is calculated to be at a SiO_2 content of about 41.5 mol%, SrO content of about 22.5 mol%, and Al_2O_3 of about 36 mol%. The log-amplitude curve shows a singularity where $g_B = 0$ m/W.

Figure 16. SIMS image of the fiber core. Relative lithium counts are on the vertical density scale on the right hand side.

Figure 17. Comparison of core optical path delay (m) at 950 nm and 1550 nm for the prototype fiber. The results suggest that the RIP at 1550 nm is 98.6% of that at 950 nm, implying small dispersion in delta-n over a wide wavelength range.

Figure 18. Brillouin gain spectrum shown at two temperatures (labeled in the graph). The dashed lines are Lorentzian fits to the data. The Brillouin frequency decreases with increasing temperature. An end-image of the cleaved fiber is provided in the inset.

Figure 19. Compositional profile for a typical Yb-doped YAG-derived fiber (Fiber 3). Yb_2O_3 concentration is ~ 0.6 mole % (~ 2.6 weight %).

Figure 20. Measured relative Raman gain spectra for the three Yb:YAG-derived fibers of the present study. Also shown is the Raman gain for pure silica. The peak Raman gain decreases with decreasing silica content. A portion of the spectrum is expanded for visual clarity. Points of interest are identified as A) ω_1, B) D_1, C) D_2, D) ω_3, E) oxygen hole centers, F) and G) ω_4.

Figure 21. Relative Raman gain (peak value) as a function of yttria+alumina content in the fibers. A line has been drawn to guide the eye. Data points are identified with their fiber number.

Figure 22. Raman gain spectra (normalized to silica) measured from the sapphire derived fiber for three different alumina concentrations. The spectrum appears to broaden and get weaker relative to the cladding (silica, black line).

Figure 23. Raman gain spectra (normalized to silica) measured from the barium oxide (BaO) derived fiber for three different baria concentrations. Several new lines appear, likely attributable to the Ba-O bond, including a strong one near 1071 cm^{-1}. The silica spectrum (black line) was obtained from the fiber cladding of one of the fibers.

Table 1. Deduced physical parameters for several oxide materials utilizing the additive model presented above.

Table 2. Summary of physical properties of the SAL fiber.

Table 3. Summary of physical properties of the LuAG-derived fiber.

Table 4. Summary of physical properties of the various glass constituents.

Table 5. Summary of optical fiber properties. Estimated or calculated values are identified while remaining values are from measurements.

Table 6. Summary of some relevant physical characteristics of lithia. Silica and alumina date from [10] are provided for comparison.

I. List of Publications Generated During This Program

This serves as a summary of the major results obtained as part of this program.

A. Journal Papers

[17] **Invited Paper.** P.D. Dragic, M.G. Pamato, V. Iordache, J. Bass, C.J. Kucera, M. Jones, T.W. Hawkins, and J. Ballato," Athermal Distributed Brillouin Sensors Utilizing All-Glass Optical Fibers Fabricated from Rare Earth Garnets: LuAG," *accepted for publication in the New Journal of Physics.*

[16] **Invited Paper.** M. Cavillon, J. Furtick, C. Kucera, C. Ryan, M. Tuggle, M. Jones, T. Hawkins, P. Dragic, and J. Ballato, "Brillouin Properties of Novel Strontium Aluminosilicate Glass Optical Fiber," *accepted for publication in the Journal of Lightwave Technology*.

[15] P.D. Dragic, C. Ryan, C.J. Kucera, M. Cavillon, M. Tuggle, M. Jones, T.W. Hawkins, A.D. Yablon, R. Stolen, and J. Ballato, "Single- and few-moded lithium aluminosilicate optical fiber for athermal Brilloiuin strain sensing," *Optics Letters*, vol. 40, no. 21, pp. 5030 – 5033 (2015).

[14] A. Ballato, P.D. Dragic, S.W. Martin, and J. Ballato, "On the anomalously strong dependence of the acoustic velocity of alumina on temperature in aluminosilicate glass optical fibers – Part II: Acoustic properties of alumina and silica polymorphs, and approximations of the glassy state," *International Journal of Applied Glass Science, in press,* DOI: 10.1111/ijag.12141.

[13] P.D. Dragic, S.W. Martin, A. Ballato, and J. Ballato, "On the anomalously strong dependence of the acoustic velocity of alumina on temperature in aluminosilicate glass optical fibers – Part I: Material Modeling and Experimental Validation," *International Journal of Applied Glass Science, in press,* DOI: 10.1111/ijag.12137.

[12] **Invited Paper**. C. Ryan, P. Dragic, J. Furtick, C. Kucera, R. Stolen, and J. Ballato, "Pockels Coefficients in Multicomponent Oxide Glasses," *International Journal of Applied Glass Science, in press,* DOI: 10.1111/ijag.12146.

[11] J. Ballato and P. Dragic, "Towards the Perfect Optical Fiber," *Journal of the South Carolina Academy of Science,* vol. 13, no. 1, pp. 9 – 12, April 2015.

[10] D. Grobnic, S.J. Mihailov, J. Ballato, and P.D. Dragic, "Type I and II Bragg gratings made with infrared femtosecond radiation in high and low alumina content aluminosilicate optical fibers," *Optica*, vol. 2, no. 4, pp. 313 – 322, 2015.

[9] P.D. Dragic, A. Mangognia, and J. Ballato, "Chirped-Fiber Brillouin Frequency-Domain Distributed Sensing," *Optical Engineering*, vol. 53, no. 5, article number 056117, 2014.

[8] **Invited Paper**. J. Ballato and P. Dragic, "Materials Development for Next Generation Optical Fiber," *Materials*, vol. 7, no. 6, pp. 4411 – 4430, 2014.

[7] **Spotlight On Optics Paper**. P. Dragic, C. Kucera, J. Ballato, K. Schuster, and D. Litzkendorf, "Brillouin Scattering Properties of Lanthano-Aluminosilicate-Core Optical Fiber," *Applied Optics,* vol. 53, no. 25, pp. 5660 – 5671, 2014.

[6] **Feature Article.** P. Dragic and J. Ballato, "120 Years of Optical Glass Science: From the Law of Mixtures to Mixing the Unmixable," *Optics and Photonics News*, vol. 25, no. 5, pp. 44 – 51, 2014.

[5] **Invited Feature Article. COVER ARTICLE.** J. Ballato and P.D. Dragic, "Rethinking Optical Fiber: New Demands, Old Glasses," *Journal of the American Ceramic Society*, vol. 96, no. 9, pp. 2675 – 2692, 2013.

[4] **Inside View.** P.D. Dragic and J. Ballato, "Characterisation of Raman gain spectra in Yb:YAG-derived optical fibres," *Electronics Letters*, vol. 49, no. 14, pp. 895 - 897, 2013.

[3] Peter D. Dragic, John Ballato, Stephanie Morris, and Thomas Hawkins, "The Brillouin gain coefficient of Yb-doped aluminosilicate glass optical fibers," *Optical Materials*, Vol. 35, no. 9, pp. 1627 - 1632, 2013.

[2] P. Dragic, C. Kucera, J. Furtick, J. Guerrier, T. Hawkins, and J. Ballato, "Brillouin spectroscopy of a novel baria-doped silica glass optical fiber," *Optics Express*, vol. 21, no. 9, pp. 10924 – 10941, 2013.

[1] A. Mangognia, C. Kucera, J. Guerrier, J. Furtick, T. Hawkins, P.D. Dragic, and J. Ballato, "Spinel-derived single mode optical fiber," *Optical Materials Express*, vol. 3, no. 4, pp. 511 – 518, 2013.

B. Conference Presentations/Papers

[14] **Invited Paper.** J. Ballato, T. Hawkins, and P. Dragic, *to be presented at ICC 2014*.

[13] **Invited Paper.** J. Ballato and P. Dragic, "Novel Brillouin- and Raman-Suppressing Optical Fibers," *IEEE Photonics Conference*, paper ThE1.1, San Diego, CA, October 12 – 16, 2014.

[12] **Invited Paper.** J. Ballato, T. Hawkins, and P. Dragic, "Novel Rare-earth Doped Optical Fibers with Intrinsically Low Brillouin and Raman Gain," *presented at the 5th International Workshop on Photoluminescence in Rare Earths: Photonic Materials and Devices (PRE '14)*, May 13 – 16, 2014, San Sebastian, Spain.

[11] J. Ballato and P. Dragic, "Brillouin-almost-free optical fibers," presented at the Fiber Society Fall Symposium, Clemson, SC, October 25, 2013.

[10] P. Dragic, J. Ballato, and T. Hawkins, "Compositional tuning of glass for the suppression of nonlinear and parasitic fiber laser phenomena," *Proc. SPIE 9081, paper 908109, 2014.*

[9] D. Grobnic, S.J. Mihailov, J. Ballato, and P.D. Dragic, "Bragg Gratings Made with IR Femtosecond Radiation in High Alumina Content Aluminosilicate Optical Fibers," *presented at Bragg Gratings, Photosensivity and Poling in Glass Waveguides (BGPP)*, paper BW2D.4, Barcelona, Spain, July 27-31 2014.
http://dx.doi.org/10.1364/BGPP.2014.BW2D.4

[8] J. Ballato, P.D. Dragic, and T. Hawkins, "Intrinsically low Brillouin- and Raman-scattering optical fibers," *Proc. SPIE*, paper 8961-42.

[7] J. Ballato, "Rethinking Optical Fiber: New Demands, Old Materials" 3rd Specialty Optical Fibers Workshop, Stockholm, Sweden, September 2013.

[6] **Invited Paper.** J. Ballato and P. Dragic, "Novel Brillouin-Suppressing Optical Fibers," presented at the Advanced Solid State Lasers (ASSL) OSA Congress, Paris, France, October 27 – November 1, 2013.

[5] J. Ballato, "Molten Core Fabrication of Novel Optical Fibers," Advanced Fibre Photonics Technologies workshop, Le Centre National de la Recherche Scientifique, Institute for Engineering and Systems Sciences (INSIS), Paris, France, October 2013.

[4] J. Ballato and P. Dragic, "Molten Core Fabrication of Novel Optical Fibers," Innovations in Glass Science and Technology - 2013 Glass and Optical Materials Division (GOMD) Meeting, Glasses for Optoelectronic and Optical Applications Symposium, 10th Pacific Rim Conference on Ceramic and Glass Technology, San Diego, CA, June 2013.

[3] **Invited Paper.** P. Dragic, "Intrinsically Low Brillouin Gain Fibers (How Low Can You Go?), presented at OSA Frontiers in Optics, Orlando FL, October 2013.

[2] P.D. Dragic, J. Ballato, S. Morris, A. Evert, R.R. Rice, and T. Hawkins, "Novel optical fibers for Brillouin-based distributed sensing," *Proc. SPIE 8722*, pp. 87220F, 2013.

[1] P.D. Dragic, J. Ballato, S. Morris, and T. Hawkins, "Intrinsically-low Brillouin gain optical fibers," *Proc. SPIE* 8733, pp. 87330N, 2013.

II. Modeling the Fiber System

The modeling approach taken in the design of intrinsically low-Brillouin-gain (ILBG) fiber compositions is not one principally meant to further the understanding of the physics of the glass systems. It is instead meant mainly to serve the following practical purposes: 1) to gain the ability to extrapolate measured fiber data from a few readily available glass compositions, 2) to develop a selection process for precursor core-phase materials, 3) to provide a way that materials science can be presented so that it is understood by fiber designers, and 4) after fabrication of a new fiber, to have a tool for the optimization of its composition. Purpose 4 clearly requires that purpose 2 be satisfied. The material additivity model requires that 1) the constituent species in an n-ary glass are separable, in that they can be treated as fully independent and 2) the constituent materials are well-mixed in the final glass, and that no anomalous effects, such as phase separation, takes place. In principle, it is not necessary for an ion (e.g., Al in Al_2O_3) to have the same coordination at every site. An additive model can provide essentially an ensemble average for the 'alumina effect' (alumina simply as an illustrative example) that can depend strongly on how and by whom the glass was fabricated. In addition, such modeling can also take into account ion-ion effects (as is typical of many phosphates [1]) such that larger binary, ternary, etc. molecules (for example large oxide molecules whose properties do not derive from their constituent oxides) can be treated as a single species. Clearly, this removes the use of the model to gain physical insight into such systems, but it can still serve as a powerful engineering tool in the design of the glass and tailored optical fibers of added value. And thus, it is for these reasons that this model is utilized in this work.

The model begins with a 'unit fiber,' as shown in Figure 1. For simplicity a binary system is first assumed, such as the ubiquitous GeO_2-doped silica glass fiber commonly found in the telecommunications industry. If the constituents of this binary system were fully separable, then one may imagine dividing the unit fiber into two independent regions of pure oxide constituent. In this case, *m* is a quantity represented as a 'length' in the Figure, but in reality is representative of the volumes occupied by the constituents. Also with respect to Figure 1, the core binary glass is well-mixed and, at least on the dimensional order much smaller than a fiber diameter or an optical or acoustic wavelength, large-scale clusters of pure material are not encountered, except perhaps where the dopant concentration is extremely small, or where such clusters are otherwise intended. While a well-mixed glass gives rise to the concept of a single optical propagation velocity, a photon 'time-of-flight' can be calculated (summed) through the separated unit fiber shown in Figure 1 to be as such

$$\Delta t = \frac{m n_1}{c} + \frac{(1-m) n_2}{c} = \frac{(m+1-m) n_{eff}}{c}. \qquad (1)$$

Then, if this time-of-flight can be lumped into the determination of an effective refractive index (right-hand side of Eqn. (1)), one can solve for the refractive index of the mixed material (dropping the subscript "eff") to be

$$n = m n_1 + (1-m) n_2 \qquad (2)$$

It is noted that Eqn. (2) also supports a thermal dependence (n(T)) incorporating a thermo-optic coefficient (*dn/dT*), if required, thereby enabling fibers with tailored *dn/dT* values for possible management of mode stability parasitics [2,3]. We have looked somewhat at this during this program, but more significantly as part of a different JTO-funded program. As stated above, *m* is

nothing more than the fractional volume of glass occupied by constituent 1. This quantity can be determined from the known composition, either in mole-, weight-, or atomic-percent, and other quantities such as the mass density, ρ (kg/m^3), and molar mass, M (g/mole). Here, the units of mole percent are adopted and one arrives at [4]

$$m = \frac{\frac{M_1}{M_2}\frac{\rho_2}{\rho_1}[C_1]}{1+[C_1]\left(\frac{M_1}{M_2}\frac{\rho_2}{\rho_1}-1\right)} \tag{3}$$

where $[C_1]$ is the concentration of the constituent #1 oxide (in mole fraction).

One can immediately see some interesting features in Eqn. (3). Understanding that the ratio M/ρ is merely the molar volume (which can depend strongly on the fiber processing history), if constituents 1 and 2 have identical molar volumes, then m is linear in $[C_1]$, and therefore the refractive index is linear in $[C_1]$. The dependence of the refractive index on [C1] is either super- or sub-linear depending on whether constituent C_1 has a molar volume that is less or greater than that of constituent 2, respectively. Essentially, this means that constituents that have a larger molar volume have a stronger effect on changing the host refractive index when in relatively low quantities than those with lower molar volume. This can serve as a selection criterion for reducing the fiber numerical aperture.

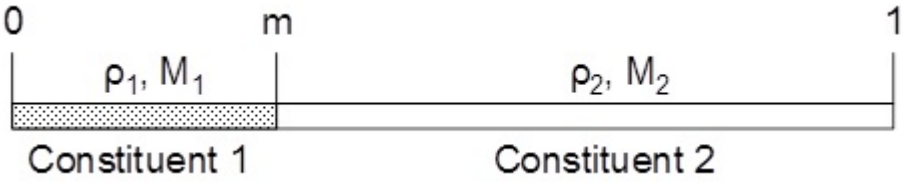

Figure 1. Representation of a unit-length fiber utilized to derive the additivity model employed in this work. This is an example of a binary, separable glass. Each constituent has its own physical properties and the volume *m* can be determined from the known composition.

An interesting feature of the additive model provided as Eqns. (2) and (3) is, once the calculations are made, the remarkable resemblance of the data to that of the mixed Sellmeier model, which utilizes six Sellmeier coefficients for each constituent. The Sellmeier model is reproduced here from [5] for convenience as

$$n^2-1=\sum_{i=1}^{3}\frac{\left[{}^{C_2}A_i+[C_1]\left({}^{C_1}A_i-{}^{C_2}A_i\right)\right]\lambda^2}{\lambda^2-\left[{}^{C_2}l_i+[C_1]\left({}^{C_1}l_i-{}^{C_2}l_i\right)\right]^2}, \tag{4}$$

where n is the index of refraction, and ${}^{C1}A$, ${}^{C1}l$, ${}^{C2}A$, and ${}^{C2}l$ are the Sellmeier coefficients for vitreous constituents 1 and 2, respectively. This will be an important point when considering the Pockels' coefficients described later.

In order to illustrate this, the case of GeO_2-doped silica is presented in Figure 2, where Eqn. (4) is plotted utilizing the coefficients found in [5], and Eqns. (2) and (3) are plotted utilizing mass densities of 2200 kg/m^3 and 3650 kg/m^3 for silica and germania, respectively. Furthermore, for the additive model, the molar masses 60.08 g/mole and 104.59 g/mole and refractive index values of 1.4442 and 1.5873, are utilized for silica and germania, respectively. The curves are very slightly sub-linear, and according to the additive model this is because the molar volume of germania is slightly higher than that of silica. More interesting than this, however, is that the curves are indistinguishable. Thus, two very different equations for the refractive index (1: Eqns. (2) and (3) based on an assumed density and refractive index; and 2: Eqn. (4) which is based on twelve empirical Sellmeier coefficients) give rise to nearly identical plots, with values that differ only starting in the 5th decimal place.

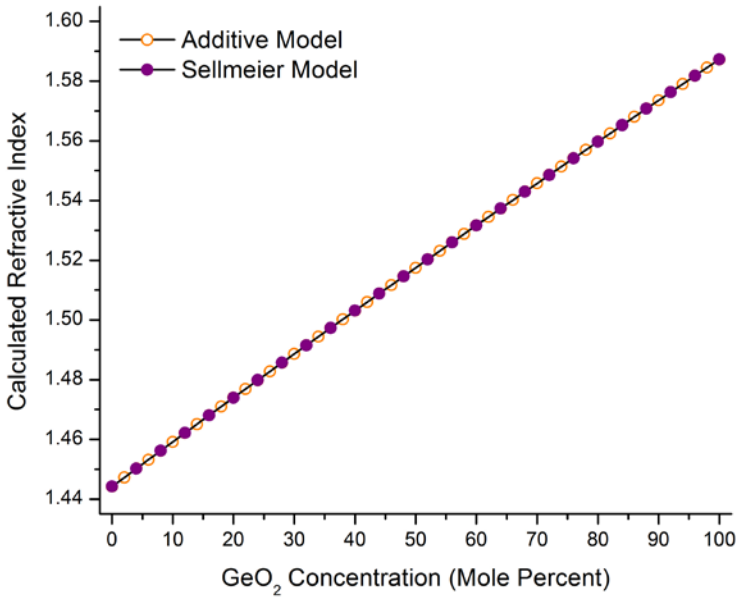

Figure 2. Plot of the refractive index of germanosilicate glass as a function of germania concentration in mole percent using both the Sellmeier and additive models (λ = 1534 nm). The graphs are indistinguishable and slightly sub-linear.

As such, the additive model can simplify the process of determining the addivity of germania and silica (and perhaps other compositions), at least with respect to the refractive index, by reducing the number of fitting terms from six to two for each component. While the density utilized for GeO_2 in the additive model (3650 kg/m^3) may not be an accurate representation of a true density of the glass network, it does allow one to design the refractive index of a germanosilicate glass; a practical consideration sought here. The bottom line for this analysis then is that the additive model can be a very trustworthy approach to designing glass, and potentially across wide compositional ranges. While processing conditions may change the observed density of a glass, and thus the resultant refractive index, these conditions and influences can be isolated and their

effect on these terms can be quantified. Thus, process-specific parameters based on changes to the draw temperature, etc. can be determined for an individual fiber maker.

The simple fiber model of Figure 1 can be employed to determine other Brillouin scattering-relevant parameters as well. Utilizing a similar time-of-flight argument for an acoustic phonon, the net acoustic velocity, V_a, can be determined [6] as can a total acoustic attenuation through the unit fiber [4]. This is accomplished by summing the attenuation in each segment (the attenuation coefficient, α, in units of m^{-1} multiplied by the length; m or [1-m] for a binary system). Multiplying the net acoustic attenuation coefficient (units of m^{-1}) by the acoustic velocity divided by π gives the Brillouin spectral width ($\Delta\nu_B$). Finally, one may also extend the model to an n-ary glass, in which case the calculations become summations over n constituents. In summary, these quantities are given by

$$V_a = \left(\sum_{i=1}^{n} \frac{m_i - m_{i-1}}{V_{a,i}} \right)^{-1} \tag{5}$$

$$\Delta\nu_B = \frac{V_a}{\pi} \sum_{i=1}^{n} \left(m_i - m_{i-1} \right) F_i\left(\nu\right) \tag{6}$$

where most typically, $F_i = (\nu/\nu_{ref})^2\alpha_i$ or that the Brillouin spectral widths of the oxide constituents are proportional to the square of the acoustic frequency ν_B [7]. Note that $m_0 = 0$ and $m_n = 1$. The subscripts i refer to the constituent number, and the m's (or rather their differences) once again are the volume content of constituent i, which can be written in terms of the molar volume and concentration in units of mole fraction. As an illustrative example, for a ternary system one obtains

$$\begin{pmatrix} m_1 \\ m_2 \end{pmatrix} = \begin{pmatrix} \left(\frac{\rho_1}{M_1}\left([C_1]-1\right) - \frac{\rho_2}{M_2}[C_1] \right) & \left(\frac{\rho_2}{M_2}[C_1] - \frac{\rho_3}{M_3}[C_1] \right) \\ \left(\frac{\rho_1}{M_1}[C_2] - \frac{\rho_2}{M_2}\left([C_2]-1\right) \right) & \left(\frac{\rho_2}{M_2}\left([C_2]-1\right) - \frac{\rho_3}{M_3}[C_2] \right) \end{pmatrix}^{-1} \bullet \begin{pmatrix} -\left(\frac{\rho_3}{M_3}[C_1] \right) \\ -\left(\frac{\rho_3}{M_3}[C_2] \right) \end{pmatrix} \tag{7}$$

where $m_0 = 0$ and $m_3 = 1$. This has since been expanded to include quaternary systems. Since the acoustic attenuation is a function of frequency, the 'quoted' acoustic attenuation α must be specified at some reference frequency, ν_{ref}. A convenient reference is 11 GHz, as this is the Brillouin scattering frequency of Corning's SMF-28™ telecommunications fiber measured at 1534 nm [4]. As a side note, in some optical fibers (such as ones produced from boria-doped silica) the acoustic attenuation is not proportional to the acoustic frequency squared [8]. This is related to the dynamic viscoelastic damping processes (and coefficients) peaking at a temperature above the glass fictive temperature, in contrast to many materials (such as silica [9])

where these processes peak at cryogenic temperatures, far from the glass fictive temperature or even T_g.

Greater detail regarding how these models are used to analyze the measured data can be found elsewhere [10,11]. However, to summarize, the additive approach has origins tracing to Winkelmann-Schott [12-14]. Starting with fused SiO_2, and its known bulk (and quenched) physical characteristics, such as mass density, refractive index, inverse of acoustic velocity [4], Brillouin spectral width (BSW), etc., material is added to the system via the most general form of the governing equation:

$$G = \sum_{i=1}^{N} g_i x_i . \qquad (8)$$

Here, x is the additivity parameter of constituent i, which in this case is the fractional volume, g is the physical property (e.g. density, refractive index, inverse of the acoustic velocity) of that constituent, and G is the aggregate value. In the case of 'mixed' glasses that form networks (such as germanosilicates), the various g's can be construed to be the bulk values of the individual constituents. For network modifiers (such as Group I or II oxides) they are likely more accurately interpreted to be their influence or change on the starting glass network, rather than some bulk value. More specifically, modeling a silicate system possessing these modifiers begins with the bulk values of the SiO_2 network, which are assumed (in approximation) to be conserved with the addition of said modifiers. Then the g values are treated as 'effective' bulk values for the network modifiers. In both cases (network formers and modifiers), once the physical properties of the fiber (which represents the aggregate glass G) are tabulated, the influences of the additional system constituents can be back-calculated.

With the mass density, ρ, also following volume additivity (as with the refractive index, Eqn. (2)), all of the quantities relevant to Brillouin gain are calculated except for the photoelastic constant, p_{12}. As a first-order approximation, this quantity may be assumed also to follow a simple additive model, as described above (e.g. Eqn. (8)). However, considering that the volume additivity model for the refractive index appears to provide excellent agreement with the Sellmeier treatment, and that the Pockels' photoelastic coefficients influence the refractive index in the case of applied stress or strain to the material, a different approach to this term was taken.

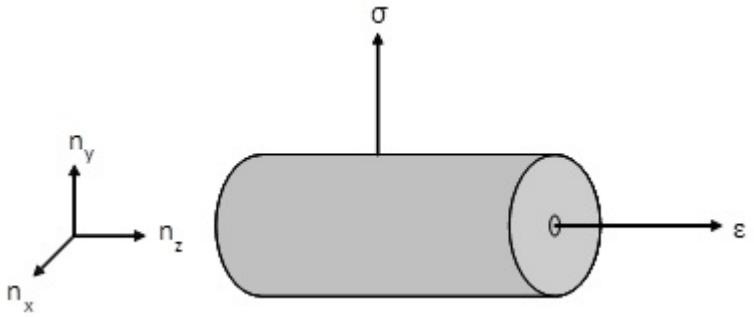

Figure 3. Block diagram providing the geometry of the system.

In the case of an applied strain, ε, an elongation of the fiber material in the longitudinal direction, z, gives rise to a change in the refractive index experienced by the transverse electric field

components (see Figure 3). Any applied strain is assumed to influence all of the individual constituents of the glass comprising the fiber (e.g., germania and silica in the case of the binary germanosilicate glass) such that the refractive index for each component becomes $n_{x,y}(\varepsilon) = n_{0,x,y} - \frac{1}{2}n_{0,x,y}^3(p_{12} - \nu(p_{11} + p_{12}))\varepsilon$ [15], where ν is the Poisson ratio and the subscript '0' corresponds to the unstrained value. In the case of an applied stress, σ', in the y-direction, a birefringence is introduced that can be found from $n_y(\sigma) - n_x(\sigma) = \frac{1}{4}(n_{0,x,y}^3/G)(p_{11} - p_{12})\sigma'$ [16,17] where G is the shear modulus and $n_{0x} = n_{0y}$ for an isotropic material. Assuming that the fiber (and thus each glass component) undergoes uniform volume deformation via the applied stress, $\sigma'/2G$ is replaced by a generalized shear deformation, σ, and thus the refractive index of the individual components (for each glass constituent) each become $n_y(\sigma) = n_{oy} - \frac{1}{2}n_{oy}^3 p_{44}\sigma$ where $p_{44} = (p_{11} - p_{12})/2$ for an isotropic material.

In summary, the assumption is made that the photoelastic constants are carried through the additive model via the refractive index. In order to simplify matters, the strain-optic coefficient, εOC, is defined to be $\varepsilon OC = p_{12} - \nu(p_{11} + p_{12})$ and the stress-optic coefficient, σOC, is defined to be $\sigma OC = (p_{11} - p_{12})/2$. The coefficients Q and P, for the strain and stress effects, respectively, are defined to be the optic coefficients multiplied by the factor: $-\frac{1}{2}n_o^3$. Applying the above set of equations to the additive model (Eqn. (8)), one obtains for a mixed binary glass that

$$\varepsilon OC_{eff}, \sigma OC_{eff} = n_0^{-3}(n_1^3 m(\varepsilon OC_1, \nu OC_1) + n_2^3(1-m)(\varepsilon OC_2, \sigma OC_2)) \qquad (9)$$

or that the strain- and stress-optic coefficients are additive with an n^3 scaling factor (n_0 is the zero-stress/strain refractive index of the net mixed glass, calculated using Eqn. (8)). Once the strain- and stress-optic components are determined, one then can solve for the individual photoelastic constants. In particular, one arrives at the following for the quantity needed in calculating the Brillouin gain

$$p_{12} = \frac{\varepsilon OC_{eff} + 2\nu\sigma OC_{eff}}{1-2\nu}. \qquad (10)$$

In [18], this model was updated and modified wherein the additivity parameters are

$$C_1' = \sum_{i=1}^{N}(m_i - m_{i-1})C_{1,i}' \qquad (11)$$

$$C_2' = \sum_{i=1}^{N}(m_i - m_{i-1})C_{2,i}' \qquad (12)$$

where $C_{1,i}' = \frac{1}{2}n_{0,i}^3(p_{12,i} - \nu_i(p_{11,i} + p_{12,i}))$ and $C_{2,i}' = \frac{1}{2}n_{0,i}^3(p_{11,i} - 2\nu_i p_{12,i})$. If we then define for the aggregate that

$$C_2' = \frac{1}{2}n_0^3(p_{12} - \upsilon(p_{11} + p_{12})) \qquad (13)$$

$$C_1' = \frac{1}{2}n_0^3(p_{11} - 2\upsilon p_{12}), \qquad (14)$$

these equations can then be solved for the p's if the Poisson ratio is known. ***In addition, another main conclusion in [18] is that through the nullification of p_{12}, the longitudinal pressure (acoustic) wave does not lead to a change in refractive index along the polarization axis of the***

optical wave, thus preventing SBS from occurring. This modified model was utilized to determine several bulk characteristics for the Group I oxides as provided in a subsequent table.

Once the physical quantities are known, the Brillouin gain may be calculated from the individual summations (that utilized Eqn. (8)).

$$g_B(\nu_B) = \frac{2\pi n^7 p_{12}^2}{c\lambda\rho V_a \Delta\nu_B} \qquad (15)$$

where once again, n is the refractive index, p_{12} is the (shear wave) photoelastic coefficient, c is the speed of light in vacuum, λ_o is the free space wavelength of the light inducing the Brillouin scattering, ρ the mass density, V_a is the acoustic velocity, and $\Delta\nu$ is the Brillouin spectral line-width. An updated table identifying these individual values for several oxide species is given in Table 1 [10,19]. ***We have found that a number of oxides contribute near-zero or negative Pockels (p_{12}) additivity when added to silica, suggesting a number of compositions where g_B = 0.***

Table 1. Deduced physical parameters for several oxide materials utilizing the additive model presented above.

Parameter	V_a	ρ	$\Delta\nu_B$**	n	p_{12}	Reference
Unit	m/s	kg/m^3	MHz	-	-	-
SiO_2	5970	2200	21	1.444	0.226	[6,20,21]
GeO_2	3510	3650	124	1.571	0.268	[21]
P_2O_5	3936	2390	177	1.488	0.255	[20,22]
B_2O_3	3315	1820	428	1.410	0.298	[23]
$Y_3Al_5O_{12}$	7649	3848	253	1.868	0.022	[24]
Al_2O_3	9790	3350	274	1.653	-0.027	[19,25]
MgO	8731	3322	*	1.810	*	[26]
SrO	3785	4015	187	1.81	-0.245	[27]
BaO	3131	4688	178	1.792	-0.33	[28]
Yb_2O_3	4110	8102	1375	1.881	-0.123	[23]
La_2O_3	3979	5676	181	1.877	-0.027	[30]
Lu_2O_3	3660	7928	145	1.66	-0.043	[31]
Li_2O	6500	3150	*	1.97	-0.01	[18,32]
Na_2O	*	3200	*	1.62	0.011	[18]
K_2O	*	2900	*	1.59	0.12	[18]

*Not yet characterized
** ν_{ref} = 11 GHz

As part of this program, we have also determined that the thermal response of Brillouin scattering can be strongly influenced by a core-cladding coefficient of thermal expansion mismatch [33,24]. Previously, the effects of thermal expansion were not included in the additive model [20,25]. Instead, the refractive index, where $n_m \rightarrow n$ (n_m is the modal index) due to the argument that the optical mode index will approximately be that of the core material value, and acoustic velocity took the forms

$$n(\varepsilon, T) = n_0 + \mathrm{TOC}\Delta T + \mathrm{SOC}\Delta\varepsilon, \quad (16)$$
$$V(\varepsilon, T) = V_0 + \mathrm{TAC}\Delta T + \mathrm{SAC}\Delta\varepsilon, \quad (17)$$

where the subscript '0' refers to the values at a control temperature (such as room temperature) and 'relaxed' mechanical state and the Δ values represent the change from those initial conditions. These equations carry through the additive model and therefore the refractive index and acoustic velocity of the binary glass may be calculated as a function of strain or temperature. If measurements of dv_a/dT are performed on a fiber, then the TAC of alumina can be deduced if the TOC (thermos-optic coefficient dn/dT) and TAC (thermo-acoustic coefficient dV/dT) of silica and the TOC of alumina are known [20]. SAC is the strain acoustic coefficient, and SOC is the strain optic coefficient, or the dependence of the acoustic velocity and refractive index on strain, respectively. It is precisely these experimentally-deduced values of the TAC from dv_a/dT measurements on several aluminosilicate-core (silica-clad) fibers that proved to be anomalously-large [35].

In order to correct the model, the assumption is made that the core is a material with larger CTE than the surrounding cladding, pure silica in the present case. Since the cladding is much more voluminous than the core, its expansion is strongly restricted by the cladding (pure silica) of the fiber, which has a thermal expansion coefficient of 0.54 x 10^{-6} K^{-1} [36]. Thus, in the longitudinal direction this restricted expansion could be likened to a negative tensile strain or positive length-wise compression of the fiber. The negative strain imparted due to the thermal expansion mismatch is taken to be $\varepsilon = -\left(\alpha_L^{core} - \alpha_L^{cladding}\right)\Delta T$, where ΔT is the change in temperature. The temperature derivative can then be found as $d\varepsilon/dT = -\left(\alpha_L^{core} - \alpha_L^{cladding}\right)$ and multiplying this by the SAC ($dV/d\varepsilon$) gives rise to a new dV/dT term.

In the radial direction, the thermal expansion mismatch imparts a positive compressive stress on the fiber. This stress can be approximated from the compressibility (inverse of the bulk modulus G) of the glass. The fractional change in volume is the pressure (P, stress) divided by G. Since the stress is in the radial direction, the change in volume can only be attributed to a stress-induced change in the cross sectional area. If the core were loose (not cladded), its area as a function of the change in temperature would be $A_{core} = \pi\left(a + \alpha_L^{core} a\Delta T\right)^2$, where a is the core diameter. Pulling the core diameter out of the equation for the area, and then expanding this expression and assuming that $2\alpha_L^{core}\Delta T \gg \left(\alpha_L^{core}\Delta T\right)^2$, the change in volume versus temperature is approximately $\frac{dVolume}{dT}\frac{1}{Volume} \approx 2\alpha_L^{core}$. Since this expansion is restricted by the cladding, the pressure (stress) on the core as a function of temperature is $\frac{dP}{dT} = 2\left(\alpha_L^{core} - \alpha_L^{cladding}\right)G$. Multiplying this by dV/dP, which can be found in the literature, gives the second correction term to dV/dT (for completeness, in units of m/(s-K)).

Therefore, to correct for the thermal expansion mismatch, Eqn. (17) is modified to

$$V(\varepsilon,T) = V_0 + \mathrm{TAC}\Delta T - \left(\alpha_L^{core} - \alpha_L^{cladding}\right)\mathrm{SAC}\Delta T + 2\left(\alpha_L^{core} - \alpha_L^{cladding}\right)G\frac{dV}{dP}\Delta T. \quad (18)$$

While the CTE mismatch also influences the refractive index, the contribution is negligible with respect to dv_a/dT when compared with that of the acoustic velocity [20,22]. As such, the modeling is assumed to be valid here, taken with $\varepsilon \rightarrow 0$ in a purely thermal setting. In Eqn. (18), each of the physical characteristics (V_0, SAC, etc.) are those of the individual constituent (silica or alumina), except for the bulk modulus G. Since the core glass is assumed to have uniform stress and/or strain, the material deformation is taken to be equivalent for both silica and alumina. In order to calculate G, first the longitudinal modulus is found from $M^L = \rho V^2$ where V and ρ are calculated using Eqn. (8). Then, the bulk modulus G is determined from

$$G = \frac{M^L(1+v)}{3(1-v)} \quad (19)$$

where the Poisson ratio v also obeys Eqn. (8).

III. Fiber Fabrication

Many of the novel compositions suggested by the model cannot be fabricated into fiber utilizing conventional methods. Instead, a 'molten core' approach is utilized, whereby one begins with a glass cladding tube and the core phase is inserted inside of it. The fiber is then drawn at a temperature above which the core phase melts and the cladding phase has softened so that it may be drawn.

The method is one that separates the consideration of core and clad as conjoined and necessarily co-processed as two glass systems. More specifically, and in some ways a return to basic glass forming, the cladding can be treated as a crucible in which the core is melted during the fiber draw process. The principal difference being that the "crucible" is an integral part of the resulting fiber and serves primarily to confine the molten core as the fiber is drawn. This 'molten core' approach, initially employing powders and termed the "power-in-tube" method, was originally applied to the fabrication of optical fibers possessing core compositions with very high rare-earth concentrations [37]. Said high rare-earth content core glasses are unstable [38] and would have devitrified had conventional optical fiber CVD processes been used.

Clearly the components of the glass (core and cladding phases) should have miscibility at the fiber processing temperature. If not, any cladding glass that enters the core region will not mix with the molten core phase, potentially leading to large optical losses in the resultant fiber. While the selection criteria for the materials described in the previous section corresponds to a 'first cut' selection, liquid-liquid miscibility is also a firm requirement for the fabrication of these fibers via the molten core process. As such, a significant effort was made in the understanding of the phase diagrams of binary, and in some cases ternary, glasses that are needed for this program. These include the BaO-SiO_2 system as an example binary glass, and the MgO-Al_2O_3-SiO_2 and BaO-Al_2O_3-SiO_2 systems as example ternary glasses (with the addition of a rare earth

resulting in a quaternary glass). Complex ternary compositions were investigated during the extension period.

IV. Summary of Optical Fibers

A. Spinel Derived Fiber

Of particular interest is the utilization of the long-studied and broadly-characterized MgO as a precursor material. Its photoelastic constant is negative and is approximately twice in magnitude than that of alumina [39], and possesses many of the other advantageous (with respect to the reduction of the Brillouin gain) properties of alumina (high density, acoustic velocity, etc.) [40]; in many ways, in fact, it is very similar to alumina. However, as its melting point is above 2800 ºC [41], MgO clad in silica represents a combination of materials not amenable to the molten core process, as the silica cladding would have already begun boiling long before the MgO melted. As such, in order to be able to characterize MgO in the context of an optical fiber dopant, a material with lower melting point was settled-upon: $MgAl_2O_4$ spinel.

From a materials perspective, "spinels" are a mineralogical class of compounds with general formula $A^{2+}B_2^{3+}O_4^{2-}$. The A and B cations occupy the octahedral and tetrahedral crystallographic sites, respectively, of the cubic lattice. The aluminum spinel, $MgAl_2O_4$, is one of the more common compositions and frequently is used as a refractory [42] and, more recently, in transparent armor [43].

Based on the guiding principles noted above, this aluminum spinel was employed as the precursor core phase in the molten core fabrication of a silica-clad magnesium aluminosilicate optical fiber [26]. As with the sapphire [25], spinel is exceedingly refractory necessitating the use of a large and thick-walled silica cladding tube. Several hundred meters of 125 μm diameter fiber was drawn at a temperature of 2175 °C, which exceeds the 2135 °C (congruent) melting point of the $MgAl_2O_4$. The resulting fiber was found to readily splice to conventional telecommunications fiber.

The resultant fibers were single-moded, a first for such intrinsically-low Brillouin gain fibers, and possessed combined MgO + Al_2O_3 concentrations between 4.5 – 5.5 weight percent. While these MgO + Al_2O_3 concentrations seem relatively low in comparison to the Al_2O_3 concentrations in the sapphire-derived fibers, they still exceed the miscibility limit in silica at conventional silica-based optical fiber processing temperatures [44]. For example, given the immiscibility of the MgO – SiO_2 system [45-47], only about 1.5 mole percent of MgO in SiO_2 would be stable at a temperature of about 1700 °C [46]. Another interesting glass structure/property feature of the spinel-derived optical fibers was that the deduced refractive index contributions from both the Al_2O_3 and MgO were higher than their respective crystalline counterparts [25,48], which may result from an effect similar to that of the SiO_2-$AlPO_4$ join [49] except resulting in an increase in refractive index.

The acoustic- and Brillouin-related features of the spinel-derived fiber were found to be both significant and useful. The spinel-derived fibers were the first truly single-mode fibers derived

from a precursor crystal and MgO was validated as increasing the acoustic velocity when added to silica, thus joining only alumina [50] and yttria [24] (and later joined by Li_2O) with this known behavior in an optical fiber. ***Further, owing to the small core diameter of the single-mode fiber and its being an acoustic anti-waveguide (since the acoustic velocity of magnesio-aluminosilicate glass is larger than that of pure silica), the Brillouin spectrum possessed the largest-reported waveguide-loss-induced spectral broadening such that, for the first time, the intrinsic Brillouin line-width of silica in fiber form was observed by direct measurement.***

The spinel-derived optical fiber, building off of the sapphire-derived analog, provided significant analytic insights while also being technologically practical. Further, in both cases, the molten core technique yielded all-glass fibers with compositions that could not have been made using conventional methods due to immiscibilities between the component phases. However, in both cases, the photoelasticity of the precursor crystal phase was not sufficiently negative such that the zero Brillouin composition was practically obtainable. As mentioned above, since pure MgO has a photoelastic constant 'only' about double that of alumina, silica concentrations as low as 10 – 20 mole % are necessary to achieve the ZeBrA condition. This leads to the baria derived fiber described in the next section.

B. BaO-Derived Optical Fibers

Upon doping into silica, barium oxide (BaO) is known to increase the binary glasses' refractive index, mass density, and as was determined [28] as part of this program, the visco-elastic damping coefficient while reducing the acoustic velocity. In addition, and like Al_2O_3, baria possesses a Brillouin frequency dependence on temperature and strain that is of opposite sign to that of silica. Hence, conceptually, both Brillouin a-thermal and a-tensic (where the Brillouin scattering frequency is independent of any applied strain on the fiber) fibers could be realized in the binary bariosilicate system; a finding previously reported for only one other glass system of practical significance: the aluminosilicates [25]. This is a disadvantage in fiber systems where heating or straining is utilized to decrease the Brillouin gain, but could prove to find great utility in distributed sensing systems.

BaO-derived all-glass optical fibers were produced by melting BaO inside a silica cladding tube [28]. The preform was drawn at a temperature of about 1975°C, which exceeds the 1920°C melting point of the baria [51] thus fulfilling the principal fabrication requirement of the molten core technique. The resultant fiber, depending upon the core size, had BaO concentrations ranging from about 23 – 37 weight percent (about 10 to 18 mole percent) in SiO_2. This fiber was also found to readily splice to conventional telecommunications fiber (see Fig. 4).

Baria, like alumina, is by no means a new material. Glass formation in the BaO-SiO_2 system has been studied as far back as 1922 [52]; and possibly earlier. Shortly thereafter, in 1927, it was known that liquid-liquid immiscibility existed between SiO_2 and the other alkaline earth oxides [46] but not initially BaO. Liquid-liquid immiscibility ultimately was identified in this binary system over the range from about 2 to 28 mole percent BaO [53]. For a more detailed discussion of the critical cooling rate, liquidus temperature, and effect of SiO_2 dissolution on BaO core melt viscosity, the reader is referred to Ref. 28. From an optical and acoustic perspective, the BaO-derived optical fiber would exhibit both a-thermal and a-tensic (in the Brillouin frequency)

compositions ***with a zero Brillouin gain condition predicted at a composition of about 33 mole percent BaO (as opposed to 88 mole percent Al_2O_3 in the sapphire-derived fiber case).*** The relative spontaneous Brillouin scattering signal from the baria-doped fiber, measured against control conventional silica optical fiber, was found to be reduced by about 10 dB in reasonable agreement with the calculated value.

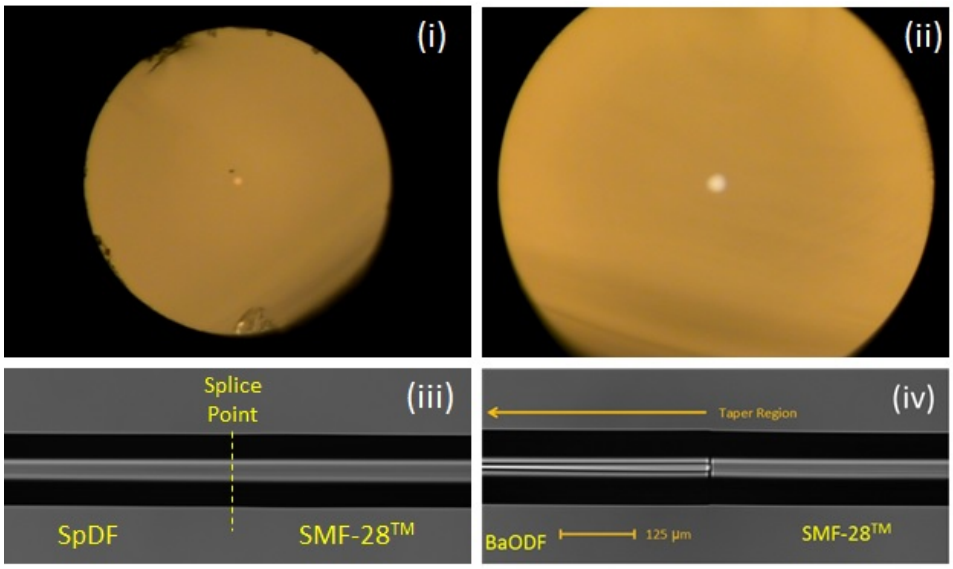

Figure 4. Optical micrograph of spinel-derived (i) and BaO-derived (ii) fiber cross-sections, splices between silica and the (iii) spinel-derived and (iv) BaO-derived fibers. In (iii) and (iv), "SpDF" refers to the spinel-derived optical fiber and "BaODF" refers to the BaO-derived optical fiber.

The observed reduction in the Brillouin gain of the fabricated fiber (~ 10 dB relative to conventional fiber) can be attributed to a large density (4688 kg/m^3), large viscoelastic damping (about twice that of alumina), and relatively large and negative photoelastic coefficient (-0.33). The latter was determined partly with the help of some data found in the literature, and thus further validation of this value is still required and is on-going. ***However, while larger than silica in magnitude [28], it is this value that enables ZeBrA fibers with more practical compositions (at about 33.5 mole% baria in silica).*** A drawback to utilizing baria as a dopant is its relatively high refractive index and low acoustic velocity relative to silica, both of which tend to increase the Brillouin gain. Since the addition of baria decreases the system acoustic velocity, and therefore also the acoustic frequency, and since the Brillouin spectral width (see Eqn. (6)) is proportional to the square of this frequency, a decreasing velocity moderates the increasing Brillouin spectral width due to visco-elastic damping [4]. This leads to the required bariosilicate composition at 20 dB Brillouin gain reduction to be relatively closer to the ZeBrA point than is needed for the aluminosilicate fiber. In fact, it is partly for this reason that the Brillouin gain for the extrapolated hypothetical pure baria is larger than that of silica. Ultimately, this is a trade-off that needs to be considered when designing the fiber laser in which the fiber will be used.

C. Rare Earth Oxides: Ytterbia

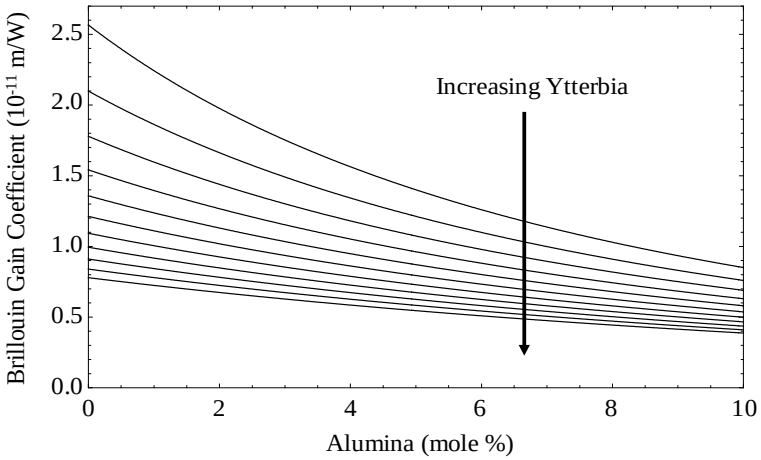

Figure 5. Brillouin gain coefficient versus alumina concentration in mole % for several ytterbia concentrations, increasing from 0 to 1 mole % (~ 6 wt%) in steps of 0.1 mol %.

We have found with a high degree of certainty that for glassy ytterbia; 1) the acoustic velocity is lower than that of silica and lower than that of ytterbia in crystalline form [54], consistent with observations for alumina; 2) ytterbia has a very large material acoustic damping coefficient, consistent with previous observations for neodymia (Nd_2O_3); and 3) the photoelastic constants are negative. Even after an extensive literature search, result #3 could not be directly corroborated with a measurement on bulk ytterbia. However the conclusion is consistent with measurements found in [55] wherein the replacement of Y^{3+} and Gd^{3+} ions with Er^{3+} ions in yttrium aluminum garnet (YAG) and gadolinium gallium garnet (GGG), respectively, resulted in both p_{11} and p_{12} being lower (typically more negative) than for their undoped counterparts. In particular only p_{12} for YAG is listed as positive, but is very small at 0.009, and decreases to -0.035 with the replacement of 26% of the Y^{3+} ions with Er^{3+} ions. In the case of GGG, replacing 15% of Gd^{3+} ions with Er^{3+} ions decreases p_{12} from -0.027 to -0.047. ***First, this suggests that bulk crystals can also exhibit ZEBRA compositions.*** Second, p_{12} in Er:YAG is less than the published value for either bulk pure alumina (-0.03) [56] or yttria (+0.057) [57] suggesting that Er_2O_3, and likely the lanthanides generally, have negative Pockels' coefficients (p_{11} and p_{12}). Finally, the self-consistency of the observed physical parameters for glassy ytterbia suggests that alumina and ytterbia can be treated as independent species within the glassy matrix. Although the mass density of ytterbia has been tied to that of alumina, inter-bonding effects, such as observed for the Al-O-P join [49], do not appear to be driving any of the observations made in this work.

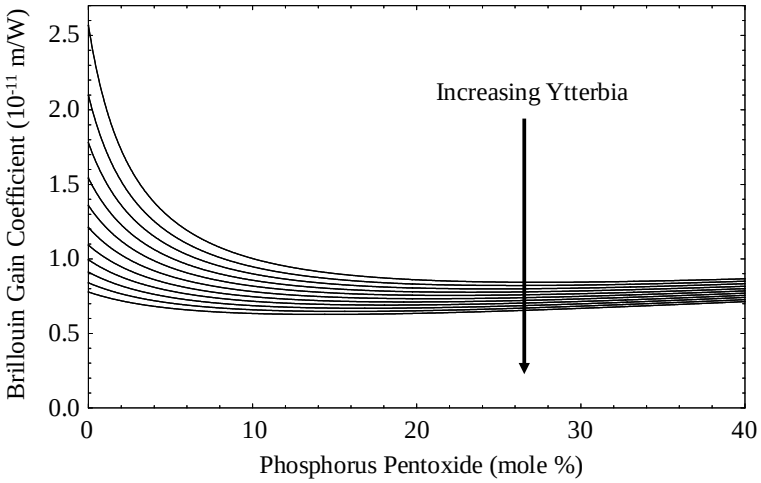

Figure 6. Brillouin gain coefficient versus P_2O_5 concentration in mole % for several ytterbia concentrations, increasing from 0 to 1 mole % (~ 6 wt%).

The higher refractive index and reduced acoustic velocity for ytterbia, relative to silica, tend to increase the BGC, while the large density, negative p_{12}, and massive Brillouin spectral width tend to decrease the BGC. In the quantities typically encountered in an active Yb-doped aluminosilicate glass (up to a few wt% of oxide), the dominant contributor to the BGC is the large material damping coefficient. Thus, even for small quantities of ytterbia, a significant reduction in the BGC can be realized relative to undoped aluminosilicate glass. To complete this section, a calculation of the BGC as a function of both ytterbia and alumina concentration are provided utilizing the parameters found in [29], with the results found in Fig. 5. The plots were extended only to realistic alumina concentrations that can be achieved utilizing conventional fiber fabrication techniques [58] to show where conventional fiber values sit.

For comparison, these calculations are extended to the Yb-doped phosphosilicate system utilizing the quantities found in [20,22], with the results provided in Fig. 6. The P_2O_5 calculations suggest that at lower concentrations there is a large degree of similarity in the BGC between the Yb-doped aluminosilicate and phosphosilicate glass systems. However, since the P_2O_5 acoustic velocity is less than that of silica, an absolute minimum in the BGC is observed, whereas for the alumina dopant, the BGC monotonically decreases. And, since the Pockels' coefficient p_{12} is negative for alumina (but is positive for P_2O_5) a zero-gain condition is reached, whereas one is not found for the P_2O_5-doped system. Access to these low-BGC aluminosilicate compositions, however, requires non-traditional methods of fiber fabrication [25]. Thus, since larger quantities of P_2O_5 can be doped into silica utilizing conventional methods, lower BGC values can be attained in 'conventional' active fibers, owing to the much larger acoustic damping coefficient when compared with silica. For example, a typical Yb-doped aluminosilicate fiber may possess 0.2 mole% of ytterbia and 5 mole% of alumina, giving rise to a BGC of about 1.1×10^{-11} m/W (for a simple step-index fiber), whereas a phosphosilicate fiber possessing 0.6 mole% of ytterbia and 20 mole% of P_2O_5 (the concentration where the BGC is minimized for the given ytterbia concentration), the BGC is about 0.7×10^{-11} m/W; a value about 2 dB lower.

D. Yb-Doped BaO-Derived Fiber

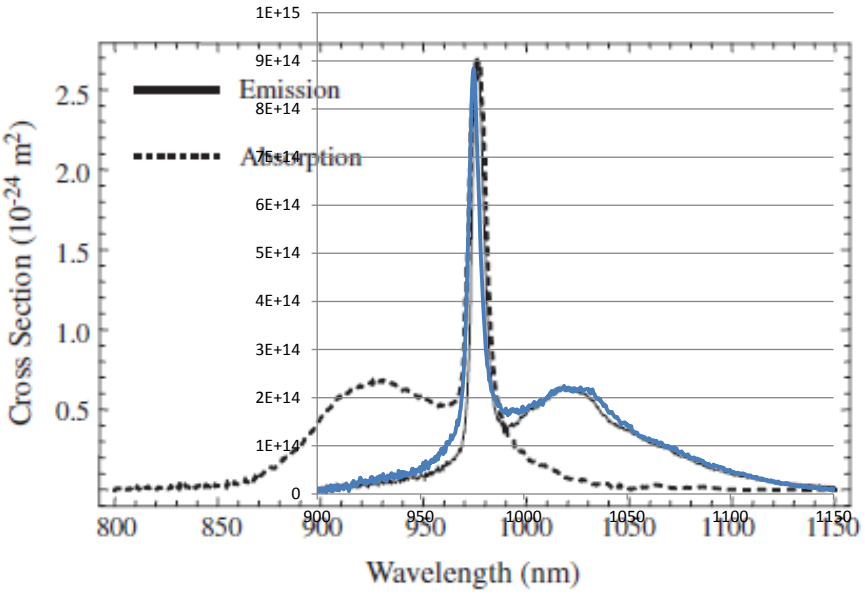

Figure 7. Overlay of the Yb-doped aluminosilicate emission spectrum (black) with that of a Yb-doped bariosilicate glass (blue). They are nearly indistinguishable.

The first group of Yb-doped BaO-derived fibers has been fabricated in this program. The ytterbia content in the fiber was somewhat high thus resulting in poor amplifier performance. However basic spectroscopy was completed with the result that Yb-doped baria-derived fibers very closely resemble their aluminosilicate counterparts (see Fig. 7). Work should continue on optimizing the precursor composition for a reduced final glass ytterbia concentration and laser measurements shall be made.

E. Lanthana Aluminosilicate Fiber

In collaboration with the Leibniz Institute of Photonic Technology, Jena, Germany, lanthana aluminosilicate (SAL) fibers were investigated [30]. To confirm the characteristics deduced for ytterbia [29], as another example of a rare earth dopant (with potentially negative p_{12}), the specific effects of lanthana (La_2O_3) on the Brillouin characteristics of silica-based oxide glass optical fibers were investigated. Lanthana is an interesting species to investigate since it possesses a wide transparency window covering the common fiber laser and telecom system wavelengths. As might be expected, it is found that the properties of lanthana are very similar to those of ytterbia (Yb_2O_3); namely low acoustic velocity, wide Brillouin spectral width, and negative photoelastic constant, with the latter two properties affording significant reductions to the Brillouin gain coefficient. However, lanthana possesses thermo-acoustic and strain-acoustic coefficients (acoustic velocity versus temperature or strain, TAC and SAC, both respectively) with signs that are opposed to those of ytterbia. The lanthano-aluminosilicate (SAL) fiber

utilized in this study is Brillouin-athermal (no dependence of the Brillouin frequency on temperature) but not atensic (is dependent upon the strain), which is believed to be, to the best of our knowledge, the first demonstration of such a glass fiber utilizing a compositional engineering approach. The Brillouin-related properties of lanthana are provided in Table 2.

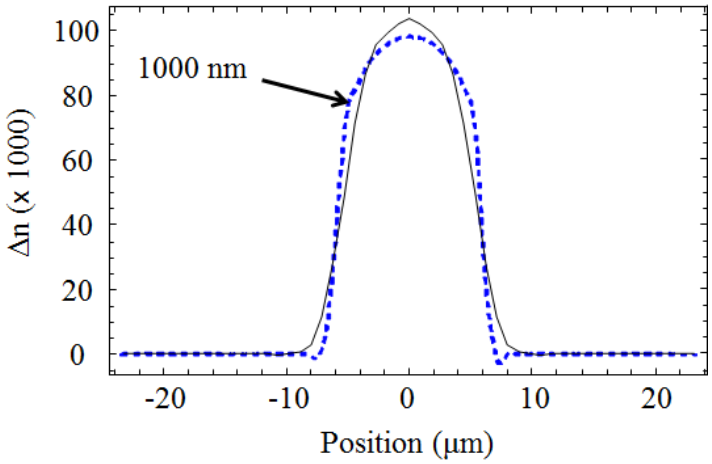

Figure 8. RIPs measured at 1000 nm and 1550 nm (the latter has a slightly higher peak Δn). The data taken at 1000 nm is shown with the dashed line.

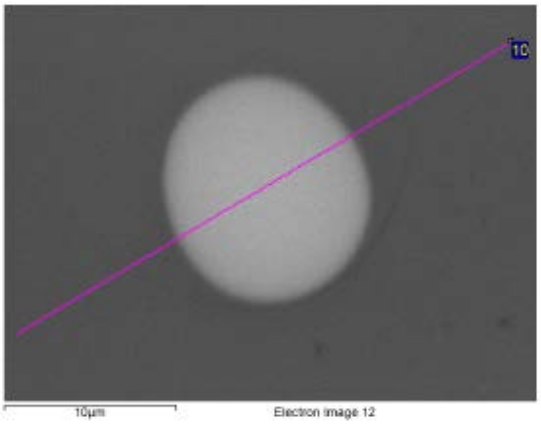

Figure 9. SEM image of the SAL fiber core. A slight ellipticity is observed.

A refractive index profile (measured at two wavelengths) and an SEM image of the fiber core are provided in Figs. 8 and 9, respectively. Due to diffusion-related processes, the core has a gradient compositional profile, with the silica content increasing moving away from the center of the core, where the composition was 11.85 mole% alumina, 9.80 mole% lanthana, and the remainder silica. To fabricate the fiber, the glass was first fabricated and then the fiber was drawn in a rod-in-tube manner. The origin of the slightly elliptical core shape is not currently known. Optical loss was approximately 2 dB/m at the measurement wavelength (1535 nm).

The experimental methodologies utilized in this study (consisting of a 'standard set' of measurements made on such novel fibers, the procedures being developed as part of this program) are identical to those found elsewhere [25,28,29], and therefore detailed descriptions will not be provided here. Instead, they are only briefly outlined as follows. The spontaneous Brillouin gain spectrum (BGS) was measured utilizing a heterodyne approach. More specifically, it was measured by launching pump power into the fiber and the resulting back-scattered signal was mixed with the pump on a fast square-law detector. The detector signal was subsequently investigated with an electrical spectrum analyzer in order to retrieve the BGS. Fibers were kept short (~ 2m) in order to minimize Brillouin spectral broadening due to any length-wise variations in the fiber. The dependence of the Brillouin frequency on temperature was measured by immersing the fiber in a thermally-controlled heated water bath. The dependence of the Brillouin frequency on strain was measured by securing a segment of the SAL fiber at both ends with epoxy. One end was affixed to a micrometer-based precision translation stage (with the other end held rigidly), from which the applied strain could be carefully measured.

The measurements of the thermo-optic and strain-optic coefficients (TOC and εOC, respectively) were achieved through the use of a ring-laser configuration. In short, the SAL fiber was placed into the cavity of a fiber ring laser operating at 1550 nm (utilizing an erbium-doped fiber as the gain medium). Since the free-spectral range of the laser is inversely proportional to the refractive index (modal), and the refractive index is a function of temperature or strain, measurements of the laser free spectral range as a function of temperature or strain disclose the TOC and εOC. Clearly this assumes that the change in length (due to thermal expansion or strain) for each of the measurements is known and measured.

The Brillouin gain coefficient is estimated by comparing the strength of the spontaneously-generated Stokes' signal with that of a fiber with known Brillouin gain. The fiber was selected so that its BGS overlaps with neither that of the apparatus (Corning SMF-28^{TM} fiber) nor that of the SAL fiber. As a result a P_2O_5-doped fiber (described in [20,22]) was utilized. The optical mode from this fiber also had good spatial overlap with the fundamental mode of the SAL fiber, such that mainly the fundamental optical mode could be excited. In mathematical terms, the Brillouin reflectivity for the two fibers were compared using the analysis in [59],

$$R_B = Ye^{G'/2}\left[I_0(G'/2) - I_1(G'/2)\right] \tag{20}$$

where I_m is the modified Bessel function of order m and

$$Y = (\bar{n}+1) g_B h\nu_S \Gamma \frac{L}{4A}, \tag{21}$$

$$G' = g_B \frac{P}{A} L, \tag{22}$$

$$\bar{n} = \left(\exp\left(\frac{h\nu_B}{kT}\right) - 1\right)^{-1}, \tag{23}$$

and where P is the pump power launched into the fiber, A is the mode effective area (determined from the mode field diameter, MFD), L is the fiber length, ν_S is the frequency of the Stokes' signal (approximately equal to that of the pump signal, at a wavelength of 1534 nm), and Γ is the decay rate ($\Gamma = \pi\Delta\nu$). The Brillouin frequency, ν_B, was selected to be the peak value from the BGS measurement. Table 2 outlines the properties measured for the fiber. Utilizing the models presented above, the values for lanthana were deduced (Table 1 in [30]).

Table 2. Summary of physical properties of the SAL fiber.

Value	Fiber 1
Optical Wavelength (nm), Brillouin Scattering Measurements	1534
Δn^* ($\times 10^{-3}$)	100
Mode Index, n_m (1534 nm); room temp. and zero strain**	1.5371
Attenuation Coefficient (dB/m) at 1534 nm	1.0
v (GHz)	11.476
V (m/s) (acoustic mode value)	5727
[Al]*** mole%	11.85
[La]*** mole%	9.80
Thermal Coefficient (MHz/K)	+0.037
TOC (K^{-1})	1.217×10^{-5}
Strain Coefficient (GHz/ε)	+16.4
εOC (unitless)	0.115
Δv (MHz)	82.0
ρ (kg/m^3)*,***	2944

*Core center value in step-wise approximation.
**Calculated from the additive model.
***Value at the core center.

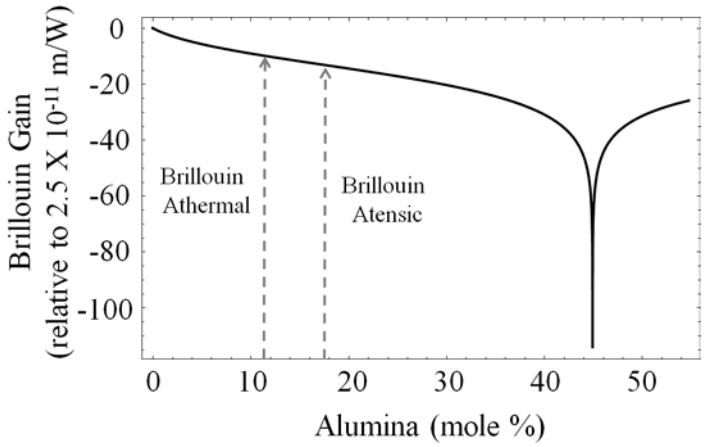

Figure 10. Brillouin gain coefficient calculated for the lanthanum aluminosilicate system (bulk) utilizing the parameters in [30] and assuming that $[Al_2O_3] = 1.21x[La_2O_3]$.

Finally, and as is relevant to this program, the Brillouin gain coefficient is provided in Fig. 10. ***It is clear that there is a wide compositional range with >20dB Brillouin gain reduction starting at about 30 mole% of alumina, with a zero-Brillouin composition appearing near 45 mole% of alumina. The assumption is that the composition be one where that $[Al_2O_3] = 1.21\times[La_2O_3]$ as***

in the present fiber. Ternary compositions such as this one provide a wide range of possible zero-Brillouin gain conditions.

F. LuAG-Derived Fiber

Two LuAG-derived fibers with different core compositions were fabricated starting with a commercial sample of LuAG ($Lu_3Al_5O_{12}$) crystal. A summary of their basic measured properties can be found in Table 3. Figure 11 shows scanning electron microscope end-images and Fig. 12 provides the measured attenuation spectra for both fibers. Several features can be seen in the spectra, and these can easily be attributed to other rare earth elements present in the starting LuAG (as well as OH absorption near 1400 nm). For example the wide features at the long-wavelength end can be attributed to Tm^{3+} and that at the short end to either Yb^{3+} or Er^{3+}. While these impurities contributed to excess loss in the fibers, they are not present in a quantity that will significantly alter the Brillouin characteristics. Fiber 1 generally has lower loss than Fiber 2 and this can probably be attributed to the core possessing a greater quantity of high-purity silica originating in the cladding. In other words, the starting core material was more diluted with a material of lower loss in Fiber 1. For completeness, it is worth noting that prior results on YAG-derived optical fibers yielded attenuation values of about 0.12 dB/m so lower losses are certainly possible [60]. The measured RIPs for the two fibers are shown in Fig. 13 and compositional data can be found in Fig. 14. Given the slight ellipticity of the fiber cores, the RIPs shown are the azimuthal averages. The graded-index shape is observed and results from the dissolutional and diffusional processes inherent to the molten core process [60]. The mode field diameter (MFD) and mode area (Petermann II method) calculated from the RIPs are also provided in Table 3.

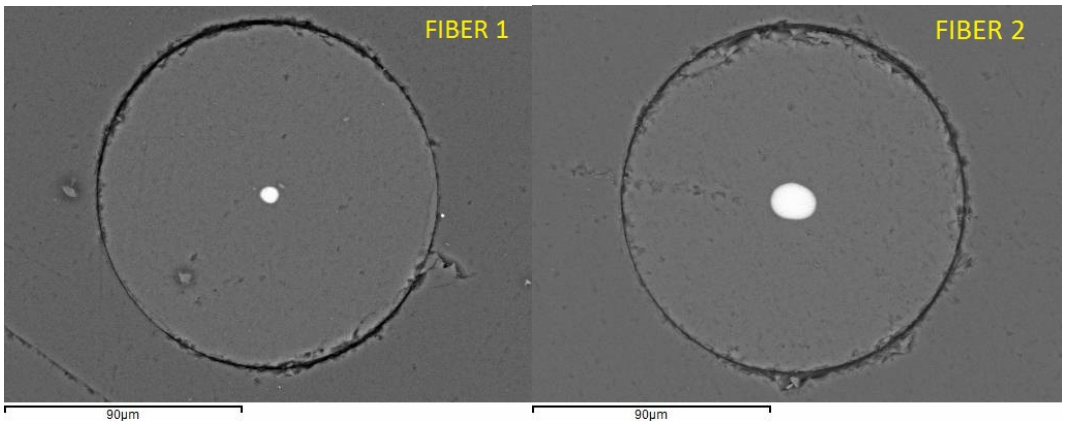

Figure 11. Scanning electron microscope end image (fiber cross section) of Fibers 1 and 2 with scale provided. There is some ellipticity in the Fiber 2 core.

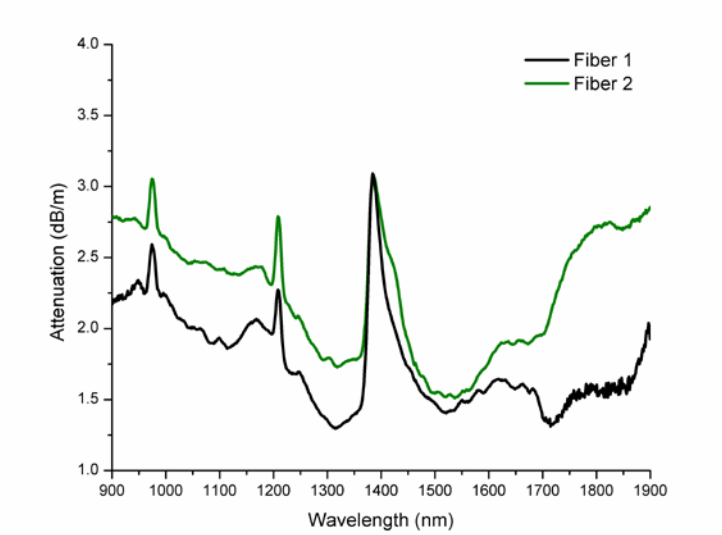

Figure 12. Attenuation spectrum for the fibers. Hydroxyl absorption near 1400 is observed. The remaining structure can be attributed to optical absorption bands of various other rare earth impurities present in the starting LuAG crystal.

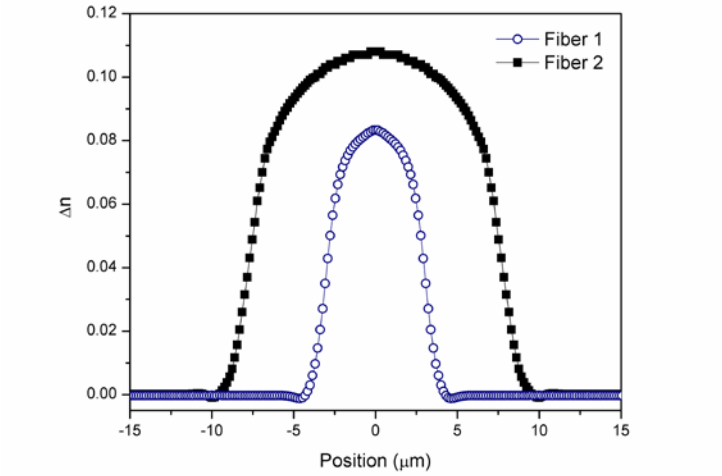

Figure 13. Refractive index profiles for Fiber 1 (open circles) and Fiber 2 (solid squares).

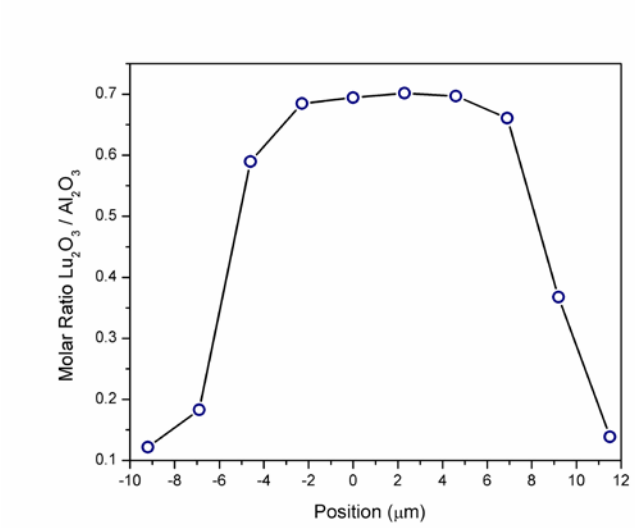

Figure 14. Molar ratio of Lu to Al across the core of Fiber 2.

Table 3. Summary of physical properties of the LuAG-derived fiber.

Value	Fiber 1	Fiber 2
Optical Wavelength (nm), Brillouin Scattering Measurements	1534	1534
Core Diameter	6.0	15
Δn^* ($\times 10^{-3}$)	83.3	108
Mode Index, n_m (1534 nm); room temp. and zero strain**	1.5108	1.5444
Mode Field Diameter, (1534 nm); room temp. and zero strain, LP_{01} mode (μm)**	4.20	6.30
Attenuation Coefficient (dB/m) at 1534 nm	1.42	1.52
ν_a (GHz)	11.347	11.574
$\Delta\nu$ (MHz)	50	65
V (m/s) (acoustic mode value)	5761	5748
$[Al_2O_3]$* mole%	7.70	11.3
$[Lu_2O_3]$* mole%	5.60	7.90
Thermal Coefficient (MHz/K)	0.269	0.065
TOC (10^{-6} K^{-1})	***	10.2
Strain Coefficient (GHz/ε)	27.9	19.5
$p_{12} - \nu_{poisson}(p_{11} + p_{12})$ (dimensionless)	***	0.123
g_B (10^{-11} m/W, peak value)	0.44 (0.63)	0.40

* Value at the core center.
**Calculated from the RIPs.
***Value could not be measured.

Another very important conclusion that can be drawn from this work is the similarity of the various rare earth sesquioxide silicates in some of their Brillouin and other material properties. For example, they universally seem to possess low (and negative) photoelastic constants and tend to have large refractive index values. Comparing Table 3 in this work and Table 1 in [30], both lanthana- and lutetia-possessing glass fibers acted very similarly with similar silica content, despite being at opposing ends of the lanthanide series.

However hidden in this similarity are some significant differences. For example, the acoustic velocity may be calculated from the Bragg condition, giving rise to the values in Table 3 for both fibers. Simple additive models may be utilized to calculate the relative contributions to the measured velocity by each of the constituent oxides. This routine has been described in detail elsewhere [10], and is somewhat simplified in the present case since both the optical and acoustic modes are confined tightly to the center of the core due to the high index [25]. As such, the measured properties of the waveguide largely take on the characteristics of the material in center, and a full waveguide analysis [20,22] becomes unnecessary. Utilizing the common theme that the density of the material drops by about 17% in going from bulk crystal to glassy phase [25], the density of Lu_2O_3 is estimated to be 7928 kg/m^3 and its acoustic velocity (longitudinal) is subsequently found to be about 3660 m/s from the fiber data. Combining this with the data for alumina used in [30], the acoustic velocity of bulk glassy $Lu_3Al_5O_{12}$ is extrapolated to be 5340 m/s. This represents a significant reduction in the acoustic velocity relative to bulk LuAG (about 25% below the measured bulk value of 7143 m/s). Given the work in [24,25], one would have expected a smaller reduction (but a reduction nonetheless) in the range of about 13%. In that case, the aggregate $Lu_3Al_5O_{12}$ constituent would have a 'glassy' acoustic velocity larger than silica, rendering an acoustic anti-waveguide, rather than a waveguide as was observed here. This demonstrates the clear utility in the characterization of oxides (among others) across the Periodic Table.

G. Strontium Aluminosilicate Fiber

Continuing along the path of the Group II oxide (barium silicates discussed above), strontium aluminosilicate fibers were developed [27]. Similar to the barium silicate fibers, the strontian content was found to be approximately 10 mole%, in addition to possessing about 17 mole% of alumina. Utilizing the complete set of data for strontium (see Table 4), along with that of alumina and silica, physical properties of the ternary glass can be calculated and predicted. Of particular interest here is the suppression of SBS, mainly through the nullification of p_{12}. In this way, the longitudinal pressure wave does not lead to a change in refractive index along the polarization axis of the optical wave [18], thus preventing SBS from occurring. As such, Fig. 15 provides the Brillouin gain coefficient, relative to a SMF fiber, as a function of SrO content, assuming a constant SrO:Al_2O_3 molar ratio of 0.6. In other words, at a SiO_2 content of zero, the glass would have a composition of 40% SrO and 60% Al_2O_3. This aluminate glass would be highly unstable and should be taken more as an extension of the model than a realizable glass composition. ***The drop to zero of the Brillouin Gain at a composition of about 41.5 mol% SiO_2 corresponds to the ZeBrA condition, where p_{12} goes to zero.*** This ZeBrA composition assumes moderately low silica content and further experiments are underway in order to achieve this composition in fiber form.

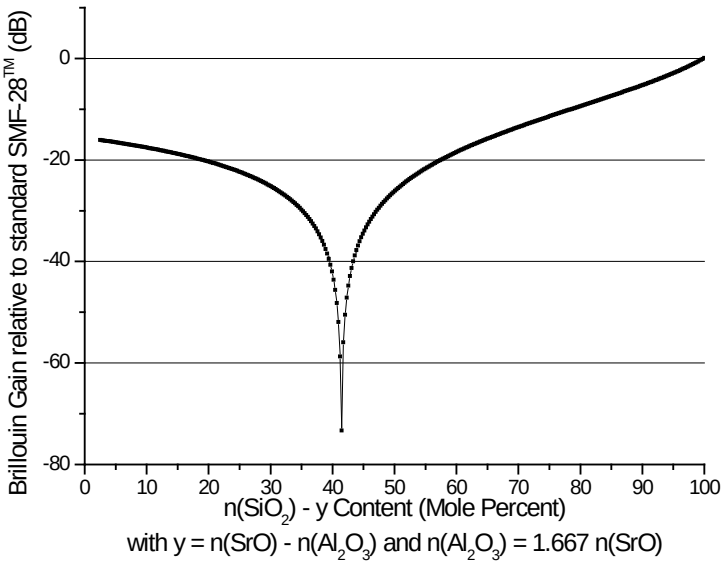

Figure 15. Calculated Brillouin coefficient (g_B) relative to a typical Ge-doped SMF versus a ratio of SiO_2-SrO-Al_2O_3 content for the ternary strontium aluminosilicate glasses. A zero-p_{12} composition is calculated to be at a SiO_2 content of about 41.5 mol%, SrO content of about 22.5 mol%, and Al_2O_3 of about 36 mol%. The log-amplitude curve shows a singularity where g_B = 0 m/W.

Table 4. Summary of physical properties of the various glass constituents.

Value	SiO_2*	Al_2O_3**	SrO	BaO***
Index (at 1534 nm)	1.444	1.653	1.810 ± 1.1%	1.7915 ± 8.0%
Molar mass (g/mol)	60.08	101.96	103.62	153.33
Density ρ (kg/m^3)	2200	3350	4015 ± 1.0%	4668 ± 0.8%
V_a(m/s)	5970	9790	3785 ± 1.6%	3131 ± 3.1%
$\Delta\nu_B$ (MHz at 11 GHz)	17.0	274	187 ± 11%	177.5 ± 2.1%
TOC (10^{-6} K^{-1})	10.4	10.5	-12.4 ± 68%	18.40 ± 6.0%
SOC	0.174	0.039	-0.120 ± 12%	-0.125 ± 47%
TAC**** (m/s/K)	+0.555	-2.41	-1.14 ± 10%	-0.390 ± 21%
SAC**** (m/s/ε)	+29.2	-46.9	-19.7 ± 9.5%	-12.007 ± 21%
p_{11}	+0.098	-0.237 ± 0.020	-0.296 ± 0.113	≈-0.33
p_{12}	+0.226	-0.027 ± 0.012	-0.245 ± 0.034	≈-0.33
Poisson Ratio	0.16	0.25	0.231 [61]	0.31

* Data from [20,22,31,62] for silica was utilized in the analysis here. Determination of the Pockels' coefficients near 15XXnm for silica can be found in [31]. The Pockels' values are somewhat lower here than in the visible wavelength range [63,64,65] due to dispersion in these parameters [31].

** Data from [25,31,35] for alumina was utilized in the analysis here. The SAC is averaged from the three fibers analyzed in [35].

*** Values for BaO provided here are taken from previous study in [28] to help the reader in the discussion.

**** TAC and SAC are the thermo-acoustic coefficient and strain-acoustic coefficient, respectively.

Novel silica-clad optical fibers possessing a SrO – Al_2O_3 – SiO_2 (SrAlSi) core were fabricated using the molten core method and their optical and Brillouin properties measured. ***The Brillouin gain coefficient of the SrAlSi fiber was found to be 0.11x10^{-11} m/W, which is about 20 times lower than conventional silica glass optical fibers.*** The SrAlSi core also exhibited a near zero Brillouin frequency thermal coefficient (-0.064 MHz/K) making it essentially athermal with respect to Brillouin frequency. These findings, taken along with those from previous work on BaO-derived optical fibers [28], suggest that Group II compounds possess intrinsically low Brillouin gain along with selected other unusual, yet useful (e.g., athermal), properties. A systematic study of MgO and CaO containing optical fibers is underway.

H. Lithium Aluminosilicate Fiber

Lithium oxide bonds into the silica glass structure as a network modifier without significant expansion of it, thereby densifying the glass. The large relative thermal expansion of lithia can be utilized as a design parameter in achieving a Brillouin-athermal single mode fiber. In order to fabricate the fiber, a starting 50:50 mol% mixture of Li_2O and Al_2O_3 powders was pressed into 3mm pellets. These pellets were utilized in a powder-in-tube molten core fabrication process [10]. A fiber was drawn down to ~ 5 μm core and standard ~ 125 μm cladding diameters from an initial 3 mm (inner diameter) x 30 mm (outer diameter) silica capillary tube preform. Fiber was drawn at 1950°C, well above the 1625°C melting point the Li_2O-Al_2O_3 composition to a length of 800 m, with the cladding diameter varying by less than 1% over the length. The purity of the precursors led to a somewhat large background loss (~ 1.75 dB/m at 1550 nm) in this proof-of-concept fiber. Reliable splicing of standard step-index telecom fiber (10 μm mode field diameter at 1550 nm; standard Corning SMF-28) to the fiber was accomplished using a built-in program on a Fitel telecom-grade portable fusion splicer. Splice losses were in the vicinity of 1 dB, mainly due to the mode-field diameter (MFD) mismatch between the fibers. Due to its low mass, lithium cannot be detected using energy dispersive X-ray spectroscopy (EDX), and instead secondary ion mass spectroscopy (SIMS) was used; initial measurements suggest ~ 6.5 mole% each of lithia and alumina in the fiber core (at core center), with the remainder being silica. Figure 16 provides the SIMS image of the fiber core while sampling ^{6}Li+. From the SIMS data, the aluminum and lithium components were found to be homogeneously mixed in the final glass. Fig. 17 provides RIP measurements, and Fig. 18 shows the Brillouin gain spectrum at two different temperatures. Table 5 provides summary data for the fiber and Table 6 gives some deduced physical properties of the Li_2O constituent.

For the very first time, we have demonstrated a silicate glass with negative Brillouin thermal response. This will have very important implications for distributed sensing applications.

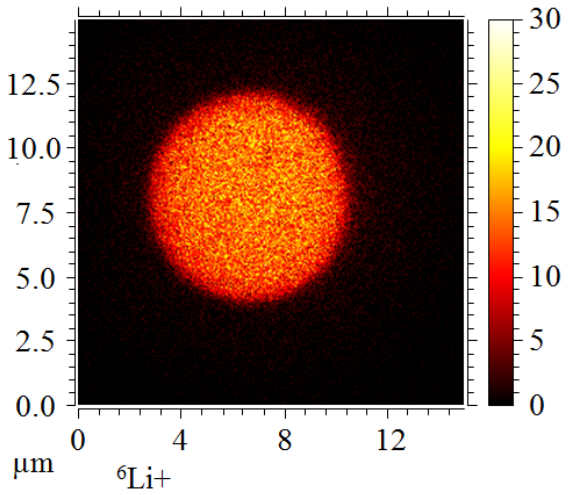

Figure 16. SIMS image of the fiber core. Relative lithium counts are on the vertical density scale on the right hand side.

Table 5. Summary of optical fiber properties. Estimated or calculated values are identified while remaining values are from measurements.

Parameter	Value
Modal Index (at 1534 nm)	1.462*
Attenuation (1550 nm, dB/m)	1.75
Core Diameter (µm)	5.3
Mode Field Diameter (1534 nm, µm)	5.17*
Alumina (core center, mole %)	6.5
Lithia (core center, mole %)	6.5
Brillouin Frequency Shift (room, temp., GHz)	11.754
Brillouin Spectral Width (room temp, MHz)	169
Acoustic Velocity (core center, m/s)	6166
Brillouin Gain Coefficient (10^{-11} m/W)	0.2**
dv/dT (MHz/K)	-0.26
dv/dε (MHz/%)	406

*calculated from RIP.
**estimated from the BGS.

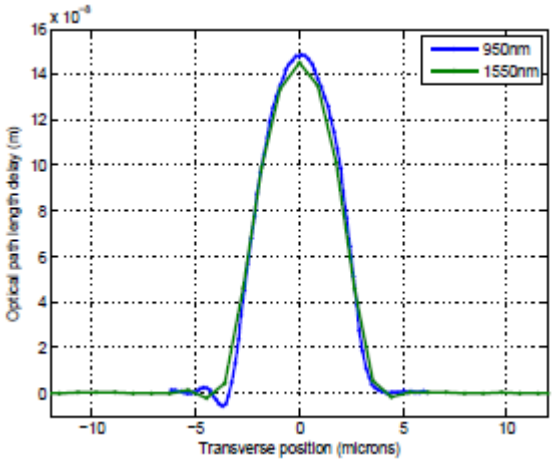

Figure 17. Comparison of core optical path delay (m) at 950 nm and 1550 nm for the prototype fiber. The results suggest that the RIP at 1550 nm is 98.6% of that at 950 nm, implying small dispersion in delta-n over a wide wavelength range.

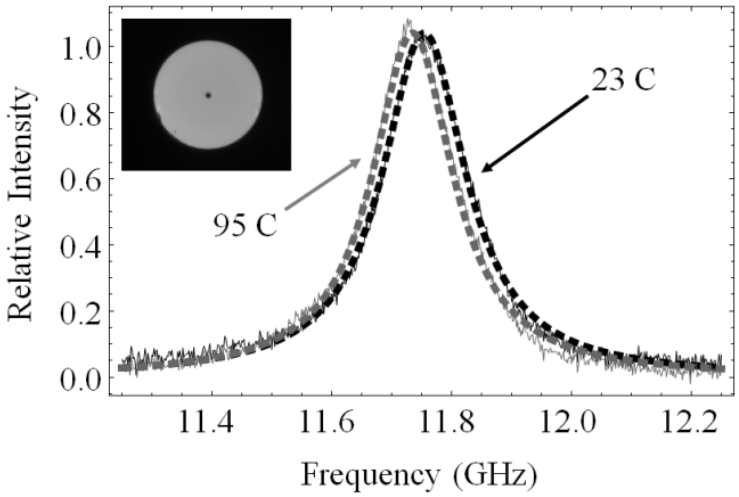

Figure 18. Brillouin gain spectrum shown at two temperatures (labeled in the graph). The dashed lines are Lorentzian fits to the data. The Brillouin frequency decreases with increasing temperature. An end-image of the cleaved fiber is provided in the inset.

Table 6. Summary of some relevant physical characteristics of lithia. Silica and alumina date from [10] are provided for comparison.

Value	SiO_2 [10]	Al_2O_3 [10]	Li_2O
Index (at 1534 nm)	1.444	1.653	1.97
Molar mass (g/mol)	60.08	101.96	29.88
Density ρ (kg/m^3)	2200	3350	3150*
Acoustic Velocity (m/s)	5970	9790	6500
p_{12}	0.252	-0.027	-0.01*
Poisson Ratio	0.16	0.25	0.086**

*Deduced from [66]. **Deduced from [67].

Lithia is found to increase the acoustic velocity when added to silica, but with magnitude less than alumina. The resulting acoustic anti-guidance, in addition to reduced value of photoelastic constant (p_{12}) causes a significant decrease in the Brillouin gain, which may be a disadvantage in distributed sensor systems via reduction in the signal-to-noise ratio if optical power is an issue. The use of higher-purity materials is expected to significantly lower the optical attenuation. Na_2O and K_2O are both expected to act in a fashion similar to that of Li_2O observed here, but both should have a greater impact on the thermal response since they influence the CTE more strongly than Li_2O [68]. They may also possess a lower acoustic velocity which could render an acoustic waveguide. Coupled with that, these materials may also prove to possess narrower intrinsic Brillouin spectral widths (lower acoustic material damping coefficients) and seem to have larger p_{12} values (see Table 1), thus greatly enhancing the Brillouin gain coefficient relative to the lithium aluminosilicate fiber presented here.

V. Investigations Into Other Compatible Fiber Improvements

Some work was done in understanding how multifunctional aspects can be engineered into fiber; i.e. simultaneously suppress SBS and other parasitic phenomena.

A. Intrinsically Low Raman Gain Glasses and Optical Fibers

The Raman spectra of several Yb:YAG-derived fibers (a typical compositional profile is provided in Fig. 19) were characterized utilizing a laser Raman microscope equipped with a laser operating at a wavelength of 785 nm (Nanophoton Corp., Raman-11). Measurements were made at the centre of the fiber core, where the concentration of silica is the least. Measurements of the pure silica spectrum were made on the claddings. Each controlled measurement utilized the same power, spot size, and duration. Thus, the relative strength of Raman scattering may be estimated from the spontaneous signal strength. Figure 20 shows the measured spectra for the three fibers,

shown with that of pure silica (cladding material). ***From the figure, it is clear that the fiber with lowest silica content also possesses the lowest Raman gain, and this reduction is roughly proportional to the silica content.*** Figure 21 provides a plot of the relative Raman gain as a function of Y_2O_3+Al_2O_3 (in units of mole %), demonstrating the approximate linearity of this relationship. Extrapolation of this line gives rise to negative gain values, and thus across a wider compositional range, the shape of this curve likely possesses some concavity.

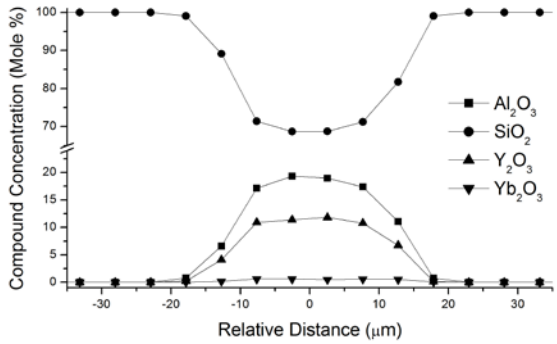

Figure 19. Compositional profile for a typical Yb-doped YAG-derived fiber (Fiber 3). Yb_2O_3 concentration is ~ 0.6 mole % (~ 2.6 weight %).

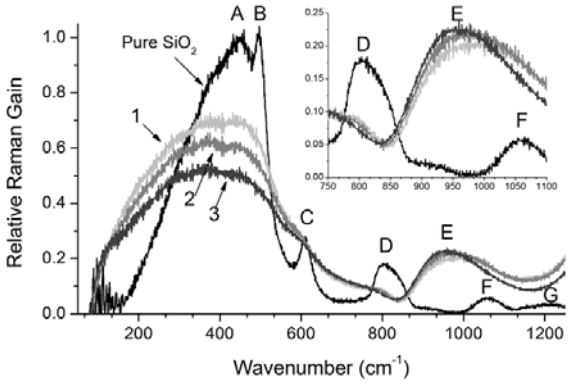

Figure 20. Measured relative Raman gain spectra for the three Yb:YAG-derived fibers of the present study. Also shown is the Raman gain for pure silica. The peak Raman gain decreases with decreasing silica content. A portion of the spectrum is expanded for visual clarity. Points of interest are identified as A) ω_1, B) D_1, C) D_2, D) ω_3, E) oxygen hole centers, F) and G) ω_4.

A relative reduction in the spontaneous Raman scattering is observed with decreasing silica content, and no Yb-related peaks are identified (owing to its low content relative to the other glass constituents). The gain reduction can partly be attributable to the replacement of (between 26.6 mole % and 32.5 mole % for the three fibers) silica with materials possessing relatively lower Raman gain. Interestingly, while other common fiber dopant materials (P_2O_5, GeO_2, B_2O_3) have Raman gain larger than that of silica [69], the measurements made here suggest that those

of alumina and yttria are lower. ***Thus, a benefit to the use of yttrium aluminosilicate with low silica content would be a reduced Raman gain and therefore increased SRS threshold.***

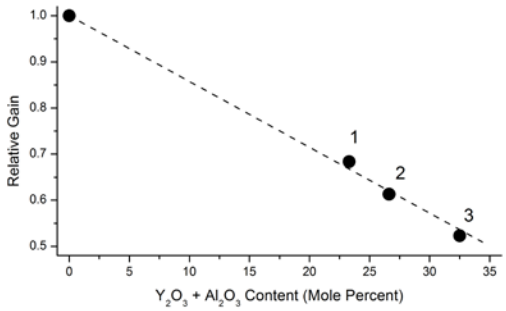

Figure 21. Relative Raman gain (peak value) as a function of yttria+alumina content in the fibers. A line has been drawn to guide the eye. Data points are identified with their fiber number.

Besides the relative reduction in the Raman gain, several interesting features of the spectra are apparent. The main peak (ω_1) near 440 cm^{-1}, attributable to the Si–O–Si stretching mode, appears to be in the same position in the YAG-derived fibers, but is much broader (~ 50% broader). This broadening may be attributable to a wider dispersion in the Si–O–Si bond angle [70] in these more highly compositionally modified glasses. The so-called defect lines at 490 cm^{-1} (D_1) and 600 cm^{-1} (D_2), attributable to 'breathing' modes of 4- and 3-member rings [71], respectively, appear to diminish considerably in the YAG-derived fiber. This may be related to a reduced fictive glass temperature [71]. However a reduced fictive temperature is usually accompanied by a reduction in the peak wave-number of the ω_1 line [71]. Since there is no apparent change in the position of this peak, it may be that the introduction of yttria and alumina to the glass network lessens the number of ring structures. However, the apparent shift in the peak near 800 cm^{-1} (bending of the Si–O bond, ω_3) does support the concept of a reduced fictive temperature; however it too appears broadened and diminished. The broadening of ω_3 may then be related also to increased dispersion in the bending angle, and perhaps a considerable amount of glass disorder possibly due to the kinetic nature of the silica (diffusing into the cladding) prior to quenching [60].

The ω_4 lines (near 1060 cm^{-1} and 1200 cm^{-1}, although most clearly visible in Fiber 1) are obscured by a new peak near 950 cm^{-1} that appears to be increasing in strength and decreasing in wave-number with decreasing silica content. The former appears to be consistent with the assignment of this band to oxygen hole centers and the broad line-widths also suggest a considerable disorder in the glass [72]. In these Yb-doped fibers, the increasing spectral intensity beyond about 1200 cm^{-1} corresponds to the onset of Yb^{3+} luminescence, and is not therefore Raman related.

Unlike Brillouin gain, Raman gain is not linked to material properties that could be potentially driven to zero by choice of composition. However, by analogy to LMA fibers where the propagating optical mode is spread out over the fiber cross-section to reduce its intensity at a given spatial location, the distribution of the glasses' bond energies can be broadened thereby reducing the effective Raman gain at a given wavelength. As described above, all-glass optical fibers derived from yttrium aluminum garnet (YAG) were fabricated [73]. It was found that the Raman peak at 440 cm^{-1}, which is associated with the Si–O–Si stretching mode, did not change position with core glass composition but was much broader spectrally likely due to a larger distribution of Si–O–Si bond angles in these more highly modified glasses. The defect line peaks at 490 cm^{-1} (D_1) and 600 cm^{-1} (D_2), which are attributable to the 4- and 3-member ring 'breathing' modes respectively, diminished with the combined (Y_2O_3 + Al_2O_3) content in the resultant glass though their spectral position did not change suggesting that yttria and alumina may lessen the number of ring structures in the glass. These same trends were also later observed for the sapphire-derived (high alumina content) fiber.

Raman spectra for the YAG-derived fibers can be found in [73] while Figure 22 shows the set of Raman spectra obtained for the sapphire-derived fiber described above. As mentioned, the features of the spectra trend in ways similar to the YAG-derived fiber. In fact, the Raman gain spectra for the YAG- and sapphire-derived fibers are nearly identical, except that the sapphire-derived fiber appears to be missing the line observed at 950 cm^{-1} (and attributed to the oxygen hole center [73]) from the YAG-derived fibers.

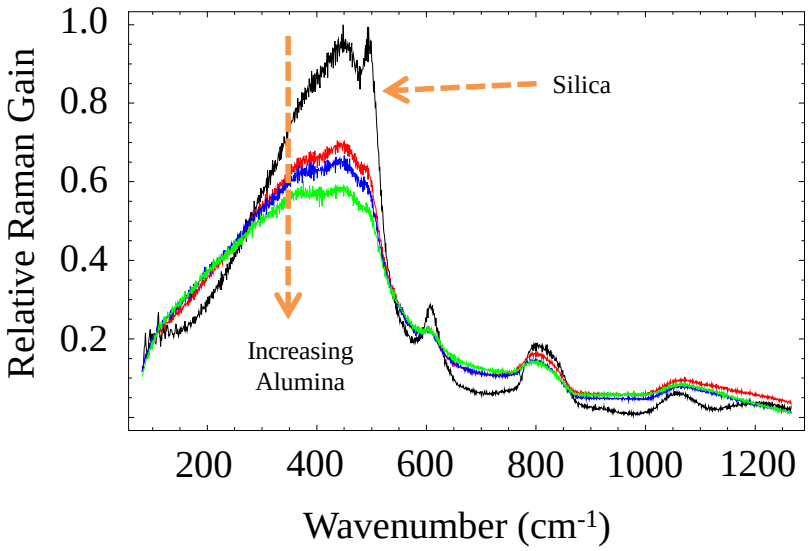

Figure 22. Raman gain spectra (normalized to silica) measured from the sapphire derived fiber for three different alumina concentrations. The spectrum appears to broaden and get weaker relative to the cladding (silica, black line).

The spectra obtained suggest that the core material possesses much more disorder than the pure silica cladding glass. As a consequence of these modifications to the glass structure, ***the spontaneous Raman scattering intensity from the yttrium-aluminosilicate fibers was found to increase linearly with increasing silica content [73] with a reduction of about 3 dB measured for a silica content of about 67.5 mol%. This trend is similar for the sapphire-derived fiber,***

with the concentrations of alumina being 26.9, 30.8, and 41.2 mol% for the three aluminosilicate fibers and a maximum reduction in Raman gain of about 2.5 dB for the highest alumina content (see Figure 22). While the reduction in Raman gain can partly be attributable to the replacement of silica with materials of relatively lower Raman gain, it is interesting to note that other common fiber dopant materials (e.g., GeO_2, P_2O_5, and B_2O_3) have Raman gain coefficients larger than that of silica. Thus, the YAG-derived fiber results highlighted here suggest that alumina and yttria impart intrinsically lower Raman gain into the glass. An additional benefit, therefore, of these low-silica content yttrium aluminosilicate glasses for optical fibers is a reduced Raman (and Brillouin) gain and therefore increased SRS (and SBS) threshold.

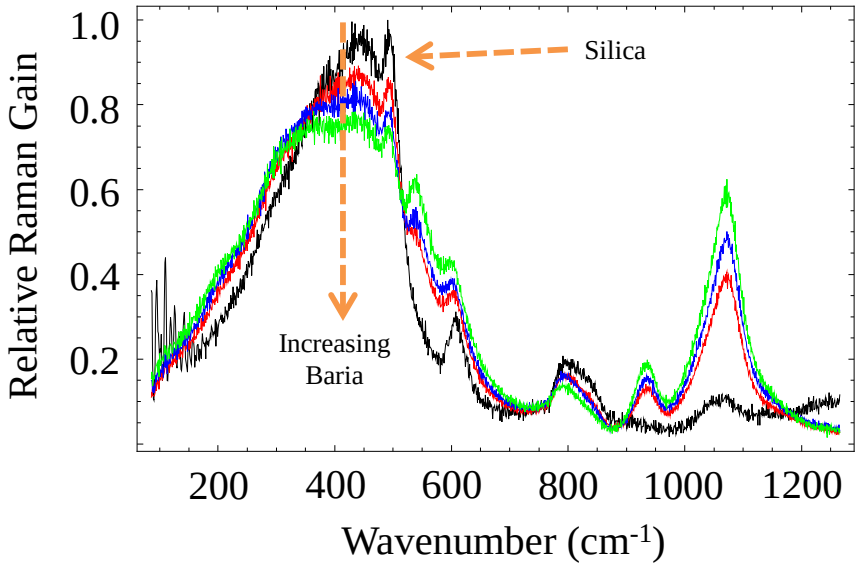

Figure 23. Raman gain spectra (normalized to silica) measured from the barium oxide (BaO) derived fiber for three different baria concentrations. Several new lines appear, likely attributable to the Ba-O bond, including a strong one near 1071 cm^{-1}. The silica spectrum (black line) was obtained from the fiber cladding of one of the fibers.

It is important to note that even with the addition of 'high-Raman-gain' materials to silica it is still possible to achieve some level of reduction to the Raman gain. As an example, the Raman spectra for the baria-derived fiber [28] are shown in Figure 23. The baria concentrations in the three fibers are 10.4, 12.3, and 18.4 mol%. Relative to the cladding spectrum (pure silica), many of the conclusions about the shape of the spectra obtained from the YAG- and sapphire-derived fiber also seem to hold for the bariosilicate fibers. However, it is also clear that several new lines appear, including a prominent one near 1071 cm^{-1} likely attributable to the Ba-O bond. From the spectra and given the concentrations of baria in the fibers, it can be deduced that the strength of the aforementioned Raman line is relatively large in the glass. In fact, one can deduce by extrapolation that at a baria concentration in the vicinity of 25–30 mol%, the Raman gain will be larger in the baria-derived fiber than that in pure silica. However, at lower BaO concentrations,

the contribution to the Raman gain spectrum by baria is at a different phonon frequency, not overlapping with a strong silica phonon line. Thus, as long as the concentration of baria is kept low enough such that its contribution to the Raman spectrum is weaker than silica, the absolute maximum Raman gain coefficient can be reduced. The bottom line is that, in the case of the bario-silicate glasses, the net Raman gain can still be reduced by up to 30% relative to silica.

B. Optical Fibers with Enhanced Thresholds for Higher Order Mode Instabilities (HOMI)

There exists in active LMA fibers a power threshold where dynamic randomization of the mode distribution at the laser output is observed, known as "higher order mode instability" (HOMI), and is believed to result from a thermally-induced refractive index grating. Since the process is believed to be driven in part by the thermo-optic coefficient (dn/dT) the natural question is whether marked increases in the HOMI threshold can be obtained through judicious tailoring of the core material's thermo-optic coefficient?

While it has already been shown that YAG-derived fibers possess larger thermal conductivities than their silica counterparts [60] (as another potential way to reduce HOMI), the material dn/dT can also be tailored. Simply stated, if $dn/dT = 0$, such modal instabilities should be improved, if not completely removed. Much like the aforementioned work on intrinsically-low-Brillouin-gain glasses, combining materials with thermo-optic coefficients of opposite sign can give rise to a significant reduction in dn/dT, and possibly even its taking on a value of zero. Materials such as SiO_2, GeO_2 (dn/dT larger than silica), and Al_2O_3 (dn/dT similar to silica) have positive dn/dT, but this value can also be negative such as in P_2O_5 and B_2O_3 [74]. ***This team is currently working on reduced dn/dT glass optical fibers through another JTO-funded program.***

C. Nonlinear Refractive Index and Parasitics Depending Thereon

Processes such as self-phase modulation (SPM) and four-wave mixing (FWM) result from the dependence of the refractive index on the optical intensity (the optical Kerr Effect). As with all other nonlinear optical processes, these may be utilized or be considered parastitics, depending on the requirements of an optical system. FWM and SPM may be useful, for example, for wavelength shifters or for generating of optical solitons, which could be useful for high bit-rate optical communications or short pulse lasers, respectively. However, their broadening and modifying of the optical spectrum may be undesirable in high peak power and multi-wavelength optical amplifier systems. The strength of these interactions is related to the nonlinear refractive index n_2, *i.e.*, to the material properties of the glass from which the fibers are made. To first order, the nonlinear index likely carries through the additive model via the refractive index (since, as mentioned above, $n(I) = n_0 + n_2 I$, where n_0 is the linear refractive index, I is the intensity of the optical signal, and n_2 is the nonlinear refractive index) much like the Pockels coefficients do through the strain and stress optic coefficients [62]. To date, however, this has not yet been verified.

There are numerous publications dedicated to the modeling of the nonlinear refractive index [75–77]. It is strongly dependent on the linear (nominal) refractive index of the material, and therefore lower refractive index materials tend to have lower n_2 values. An expression for n_2

in terms of widely used glass engineering coefficients, e.g., the Abbe number v_d and the refractive index at the Fraunhofer d-line, is [75]

$$n_2(esu) = \frac{K(n_d - 1)(n_d^2 + 2)^2}{v_d\sqrt{1.517 + (n_d^2 + 2)(n_d + 1)\frac{v_d}{6n_d}}} \quad (24)$$

where K is a material constant that is dependent upon the effective oscillator strength (or strength of the induced dipole moment) and shape of the potential well of the oscillator [75]. Upon inspection it is seen that materials with large Abbe numbers and low n_d are desirable for achieving low nonlinear refractive index values. As a result, classes of fluoride glasses, for example, have relatively low n_2 [77]. Unfortunately, the ranges of Abbe numbers and refractive indices available for most common glass-forming materials are limited (perhaps 50–100 for the former and 1.4 to 1.6 for the latter), and the effectiveness of reducing n_2 in this way is therefore also limited. Of perhaps greater interest is that heretofore a more 'chemical' approach may be taken in the design of materials with predetermined n_2. The nonlinear refractive index depends strongly on the polarizability of the material and, therefore, on the nature of the chemical bond (which strongly influence the parameter K). It has been found that in some covalent bonding systems, in contrast to ionic ones, the value of n_2 (via K [75]) might even take on negative values [78]. Therefore, if an abundance of covalent bonds can be engineered into the material, for example the Al-O-P bond in the $AlPO_4$ system [49], significant reductions in n_2 may be possible. This work has only just begun but offers exciting possibilities to control n_2-based nonlinearities. We note that this may also be a path to reduction of the *linear* refractive index and thus the NA of the fiber core.

VI. Future Work

To keep this section brief, we first point out that a powerful fiber fabrication process, coupled with meticulous measurements and modeling, has disclosed a vast array of material possibilities possessing a wide range of performance characteristics, including zero SBS, reduced Raman, sensing-enhanced fibers, etc. Of particular importance to the high-power fiber laser application are reduced deleterious effects of nonlinear parasitics (fibers with suppressed Brillouin and Raman gain, and n_2). We have shown that a large number of ZeBrA compositions appear to be possible (although we have not yet been able to demonstrate a ZeBrA composition), and the range of value-added compositions broadens considerably if 20dB Brillouin gain reduction is taken to be the requirement.

Regarding Brillouin scattering, it was found that the most promising materials are the Group II and lanthanide (rare earth) oxides (+ alumina). Future work would include the development of such silicate materials into active fibers for high power operation. Lanthanides (+ alumina) also offer the added benefit of reducing the Raman gain coefficient. n_2 would still need to be characterized for these glass systems. However, a path towards the perfect optical fiber, one which simultaneously possesses the aforementioned low-nonlinearity attributes, becomes well defined and well-within reach. Designing fibers to possess a lower numerical aperture would require incorporating an index-reducing material (such as F or B_2O_3), thus coupled with the

active ion, rendering necessary quaternary or quinary glasses, which can all be fabricated utilizing the methodology outlined here.

VII. References

[1] R. Shannon, R.C. Shannon, O. Medenbach, and R.X. Fischer, "Refractive Index and Dispersion of Fluorides and Oxides," J. Phys. Chem. 31, 931 – 970 (2002).

[2] K. Hansen, T. Alkeskjold, J. Broeng, and J. Lægsgaard, "Theoretical analysis of mode instability in high-power fiber amplifiers," Opt. Express 21, 1944 – 1971 (2013).

[3] C. Jauregui, T. Eidam, H. Otto, F. Stutzki, F. Jansen, J. Limpert, and A. Tünnermann, "Physical origin of mode instabilities in high-power fiber laser systems," Opt. Express 20, 12912 – 12925 (2012).

[4] P. Dragic, "Simplified model for effect of Ge doping on silica fibre acoustic properties," Electron. Lett. 45, 256 – 257 (2009).

[5] J. Fleming, "Dispersion in GeO_2—SiO_2 glasses," Appl. Opt. 23, 4486 – 4493 (1984).

[6] P. Dragic, "The Acoustic Velocity of Ge-Doped Silica Fibers: A Comparison of Two Models," Int. J. Appl. Glass Sci. 1, 330 – 337 (2010).

[7] G. Agrawal, *Nonlinear Fiber Optics* (Academic Press, New York, 1995).

[8] P. Law and P. Dragic, "Wavelength dependence of the Brillouin spectral width of boron doped germanosilicate optical fibers," Opt. Express 18, 18852 – 18865 (2010).

[9] A. Pine, "Brillouin scattering study of acoustic attenuation in fused quartz," Phys. Rev. 185, 1187–1193 (1969).

[10] J. Ballato and P. Dragic, "Rethinking Optical Fiber: New Demands, Old Glasses," *J. Am. Ceram. Soc*., vol. 96, no. 9, pp. 2675 – 2692, Aug. 2013.

[11] P. D. Dragic, "The Acoustic Velocity of Ge-Doped Silica Fibers: A Comparison of Two Models," *Int. J. Appl. Glass Sci.*, vol. 1, no. 3, pp. 330 – 337, Aug. 2010.

[12] A. Winkelmann and O. Schott, "Über die Elastizität und über die Zug- und Druckfestigkeit verschiedener neuer Gläser in ihrer Abhängigkeit von der chemischen Zusammensetzung [On the elasticity and the tensile and compressive strength of several new glasses in their dependence on the chemical composition],"*Annalen der Physik.*, vol.287, no. 4, pp. 697 – 730, 1894.

[13] A. Winkelmann and O. Schott, "Über thermische Widerstandscoefficienten verschiedener Gläser in ihrer Abhängigkeit von der chemischen Zusammensetzung [On the thermal resistance coefficients of different glasses in their dependence on chemical composition],"*Annalen der Physik.*, vol. 287, no. 4, pp. 730 – 746, 1894.

[14] A. Winkelmann, “Ueber die Elasticitätscoefficienten verschieden zusammengesetzter Gläser in ihrer Abhängigkeit von der Temperatur [On the elastic coefficients of different composite glasses in their dependence on the temperature],”*Annalen der Physik.*, vol.297, no. 5, pp. 105 – 141, 1897.

[15] C. Butter and G. Hocker, “Fiber optics strain gauge,” Appl. Opt. 17, 2867 – 2869 (1978).

[16] K. Matusita, C. Ihara, T. Komatsu, and R. Yokota, “Photoelastic Effects in Silicate Glasses,” J. Am. Ceram. Soc. 67, 700 – 704 (1984).

[17] M. Huang, “Stress effects on the performance of optical waveguides,” Int. J. Sol. Struct. 40, 1615 – 1632 (2003).

[18] C. Ryan, P. Dragic, J. Furtick, C. Kucera, R. Stolen, and J. Ballato, “Pockels Coefficients in Multicomponent Oxide Glases,” *International Journal of Applied Glass Science, in press,* DOI: 10.1111/ijag.12146.

[19] J. Ballato and P. Dragic, “Materials Development for Next Generation Optical Fiber,” *Materials* 7(6), 4411 – 4430 (2014).

[20] P. Law, Y. Liu, A. Croteau, and P. Dragic, “Acoustic coefficients of P_2O_5-doped silica fiber: acoustic velocity, acoustic attenuation, and thermo-acoustic coefficient,” Opt. Express 1, 686 – 699 (2011).

[21] P. Dragic and B. Ward, “Accurate modeling of the intrinsic Brillouin linewidth via finite element analysis,” IEEE Photon. Technol. Lett. 22, 1698 – 1700 (2010).

[22] P. Law, A. Croteau, and P. Dragic, “Acoustic coefficients of P_2O_5-doped silica fiber: the strain-optic and strain-acoustic coefficients,” Opt. Mat. Express 2, 391 – 404 (2012).

[23] P. Dragic, “Brillouin Gain Reduction Via B_2O_3 Doping,” J. Lightwave Technol. 29, 967 – 973 (2011).

[24] P. Dragic, P.-C. Law, J. Ballato, T. Hawkins, and P. Foy, “Brillouin Spectroscopy of YAG-Derived Optical Fibers,” Opt. Express 18, 10055 – 10067 (2010).

[25] P. Dragic, T. Hawkins, S. Morris, and J. Ballato, “Sapphire-derived all-glass optical fibers,” Nature Photon. 6, 629 - 635 (2012).

[26] A. Mangognia, C. Kucera, J. Guerrier, J. Furtick, P. Dragic, and J. Ballato, “Spinel-Derived Single Mode Optical Fiber,” Opt. Mater. Express 3, 511 – 518 (2013).

[27] M. Cavillon, J. Furtick, C. Kucera, C. Ryan, M. Tuggle, M. Jones, T. Hawkins, P. Dragic, and J. Ballato, “Brillouin Properties of Novel Strontium Aluminosilicate Glass Optical Fiber,” *accepted for publication in the Journal of Lightwave Technology.*

[28] P. Dragic, C. Kucera, J. Furtick, J. Guerrier, T. Hawkins, and J. Ballato, “Brillouin Spectroscopy of a Novel Baria-doped Silica Glass Optical Fiber,” *Optics Express,* vol. 21, no. 9, pp. 10924 – 10941, 2013.

[29] P. Dragic, J. Ballato, S. Morris, and T. Hawkins, “The Brillouin gain coefficient of Yb-doped aluminosilicate glass optical fibers,” Opt. Mater. (in press 2013).

[30] P. Dragic, C. Kucera, J. Ballato, K. Schuster, and D. Litzkendorf, “Brillouin Scattering Properties of Lanthano-Aluminosilicate-Core Optical Fiber,” Opt. Mater. Express 53, 5660 – 5671 (2014).

[31] P.D. Dragic, M.G. Pamato, V. Iordache, J. Bass, C.J. Kucera, M. Jones, T.W. Hawkins, and J. Ballato,” Athermal Distributed Brillouin Sensors Utilizing All-Glass Optical Fibers Fabricated from Rare Earth Garnets: LuAG,” *accepted for publication in the New Journal of Physics*.

[32] P.D. Dragic, C. Ryan, C.J. Kucera, M. Cavillon, M. Tuggle, M. Jones, T.W. Hawkins, A.D. Yablon, R. Stolen, and J. Ballato, “Single- and few-moded lithium aluminosilicate optical fiber for athermal Brilloiuin strain sensing,” *Optics Letters*, vol. 40, no. 21, pp. 5030 – 5033 (2015).

[33] A. Ballato, P.D. Dragic, S.W. Martin, and J. Ballato, “On the anomalously strong dependence of the acoustic velocity of alumina on temperature in aluminosilicate glass optical fibers – Part II: Acoustic properties of alumina and silica polymorphs, and approximations of the glassy state,” *International Journal of Applied Glass Science, in press*, DOI: 10.1111/ijag.12141.

[34] P.D. Dragic, S.W. Martin, A. Ballato, and J. Ballato, “On the anomalously strong dependence of the acoustic velocity of alumina on temperature in aluminosilicate glass optical fibers – Part I: Material Modeling and Experimental Validation,” *International Journal of Applied Glass Science, in press,* DOI: 10.1111/ijag.12137.

[35] P. Dragic, J. Ballato, A. Ballato, S. Morris, T. Hawkins, P.-C. Law, S. Ghosh, and M.C. Paul, “Mass density and the Brillouin spectroscopy of aluminosilicate optical fibers,” Opt. Mat. Express **2**, 641 – 1654 (2012).

[36] "Selecting Thermal Properties," in *CRC Materials Science and Engineering Handbook, Third Edition*, J. Shackelford and W. Alexander, eds. (CRC Press, 2010), pp. 1540.

[37] J. Ballato and E. Snitzer, “Fabrication of Fibers with High Rare-Earth Concentrations for Faraday Isolator Applications,” Appl. Opt. 34, 6848 – 6854 (1995).

[38] A. Makishima, M. Kobayashi, and T. Shimohira, ‘‘Formation of aluminosilicate glasses containing rare-earth oxides,’’ J. Am. Ceram. Soc. 65, C-210 (1982).

[39] K. Rao and V. Murty, “Photoelastic constants of magnesium oxide,” Acta Cryst. 17, 788 – 789 (1964).

[40] N. Soga and O. Anderson, “High-Temperature Elastic Properties of Polycrystalline MgO and Al_2O_3,” J. Am. Ceram. Soc. 49, 355 – 359 (1966).

[41] C. Ronchi and M. Sheindlin, “Melting point of MgO,” J. Appl. Phys. 90, 3325 – 3331 (2001).

[42] *Refractories Handbook*, Charles Schacht, editor (CRC Press, 2004); ISBN 0203026322.

[43] J. Swab, J. Lasalvia, G. Gilde, P. Patel, and M. Motyka, “Transparent Armor Ceramics: AlON and Spinel,” in *23rd Annual Conference on Composites, Advanced Ceramics, Materials, and Structures: B*; Ceramic Engineering and Science Proceedings, Volume 20 Issue 4, E. Ustundag and G. Fischman, editors, (John Wiley & Sons, Inc., Hoboken, NJ, USA, 2008).

[44] G. Rankin and H. Merwin, "The Ternary System MgO – Al_2O_3 – SiO_2," Am. J. Sci. 45, 301 – 325 (1918).

[45] N. Bowen and O. Andersen, "The Binary System MgO – SiO_2," Am. J. Sci. 37, 487 – 500 (1914).

[46] J. Greig, "Immiscibility in Silicate Melts; Part I," Am. J. Sci. 13, 1 – 44 (1927).

[47] P. Wu, G. Eriksson, A. Pelton, and M. Blander, "Prediction of the Thermodynamics Properties and Phase Diagrams of Silicate Systems – Evaluation of the FeO – MgO – SiO_2 System," ISIJ Int. 33, 26 – 35 (1993).

[48] J. Heaney, G. Hass, and M. McFarland, "Spinel (Al_2O_3:MgO): refractive-index variations and lack of stoichiometry in evaporated films," Appl. Opt. 20, 2335 – 2336 (1981).

[49] D. DiGiovanni, J. MacChesney, and T. Kometani, "Structure and properties of silica containing aluminum and phosphorus near the $AlPO_4$ join," J. Non-Cryst. Sol. 113, 58 – 64 (1989).

[50] C. Jen, C. Neron, A. Shang, K. Abe, L. Bonnell, and J. Kushibiki, "Acoustic Characterization of Silica Glasses," J. Am. Ceram. Soc. 76, 712 – 716 (1993).

[51] M. Huntelaar and E. Cordfunke, "The ternary system $BaSiO_3$-$SrSiO_3$-SiO_2," J. Nucl. Mater. 201, 250 – 253 (1993).

[52] P. Eskola, "The silicates of strontium and barium," Am. J. Sci. 4, 331 – 375 (1922).

[53] T. Seward, D. Uhlmann, and D. Turnbull, "Phase Separation in the System BaO-SiO_2," J. Am. Ceram. Soc. 51, 278 – 285 (1968).

[54] B.R. Powell, Jr., O. Hunter, Jr., and W.R. Manning, "Elastic Properties of Polycrystalline Ytterbium Oxide," *J. Am. Ceram. Soc*., vol. 54, pp. 488 – 490, 1971.

[55] V.F. Kitaeva, N.N. Sobolev, I.L. Chistyĭ, E.V. Zharikov, V.V. Osiko, M.I. Timoshechkin, and A.S. Zolot'ko, "Molecular scattering of light in erbium-doped garnets," *Sov. Phys. Solid State*, vol. 22, no. 5, pp. 805 – 807, May 1980.

[56] H. Eilers, E. Strauss, and W.Yen, "Photoelastic Effect in Ti^{3+}-doped Sapphire," *Phys. Rev. B*, vol. 45, pp. 9604 – 9610, 1992.

[57] V.I. Aleksandrov, V.F. Kitaeva, V.V. Osiko, N.N. Sobolev, V.M Tatarintsev, and I.L Chistyi, "Spectra of molecular scattering of light in Y_2O_3 and Sc_2O_3 crystals," Soviet Physics - Lebedev Institute Reports, Number 4, pp. 7 – 13, 21 November, 1975.

[58] J. Simpson and J. MacChesney, "Optical Fibres with an Al_2O_3-Doped Silicate Core Composition," *Electron. Lett*., vol. 19, pp. 261 – 262, 1983.

[59] R.W. Boyd, K. Rzażewski, and P. Narum, "Noise initiation of stimulated Brillouin scattering," Phys. Rev. A **42**, 5514 – 5521 (1990).

[60] J. Ballato, T. Hawkins, P. Foy, B. Kokuoz, R. Stolen, C. McMillen, M. Daw, Z. Su, T. M. Tritt, M. Dubinskii, J. Zhang, T. Sanamyan, and M. J. Matthewson, "On the fabrication of all-glass optical fibers from crystals," J. Appl. Phys. **105**(5), 053110 (2009).

[61] B. Ghebouli, M. A. Ghebouli, M. Fatmi, and M. Benkerri, "First-principles calculations of structural, elastic, electronic and optical properties of XO (X = Ca, Sr, and Ba) compounds under pressure effect," *Mater. Sci. Semicond. Process*., vol. 13, no. 2, pp. 92 – 101, Apr. 2010.

[62] P. Dragic, J. Ballato, S. Morris, and T. Hawkins, "Pockels' Coefficients of Alumina in Aluminosilicate Optical Fiber," J. Opt. Soc. Am. B 30, 244 – 250 (2013).

[63] T. Horiguchi, T**.** Kurashima, and M. Tateda, "Tensile strain dependence of Brillouin frequency shift in silica optical fibers," *IEEE Photon. Technol. Lett.*, vol. 1, no. 5, pp. 107 –109, May 1989.

[64] A. D. Yablon, M. F. Yan, P. Wisk, F. V. DiMarcello, J. W. Fleming, W.A. Reed, E. M. Monberg, D. J. DiGiovanni, J. Jasapara, and M. E. Lines, "Refractive index perturbations in optical fibers resulting from frozen-in viscoelasticity," *Appl. Phys. Lett*., vol. **84**. No. 1 pp. 19-21, 2004.

[65] M. J. Weber, *Handbook of optical materials*, The CRC Press laser and optical science and technology series (CRC Press, 2003), supplement optical glasses, Sec.2

[66] J. Schroeder, "Brillouin scattering and Pockels coefficients in silicate glasses, "J. Non-Cryst. Sol. **40**, pp. 549 – 566, 1980.

[67] R. Dovesi, C. Roetti, C. Freyria-Fava, M. Prencipe, and V.R. Saunders, "On the elastic properties of lithium, sodium and potassium oxide. An ab initio study," Chem. Phys. **156**, pp. 11 – 19, 1991.

[68] H.F. Shermer, "Thermal Expansion of Binary Alkali Silicate Glasses," J. Res. Nat. Bur. Stand. **57**, 2698, 1956.

[69] Galeener, F.L., Mikkelsen, J.C., Geils, R.H., and Mosby, W.J.: 'The relative Raman cross sections of vitreous SiO_2, GeO_2, B_2O_3, and P_2O_5', *Appl. Phys. Lett.*, 1978, **32**, pp. 34 – 36.

[70] Martinet, C., Martinez, V., Coussa, C., Champagnon, B., and Tomozawa, M., 'Radial distribution of the fictive temperature in pure silica optical fibres by micro-Raman spectroscopy', *J. Appl. Phys.*, 2008, **103**, pp. 083506.

[71] Galeener, F.L.: 'Raman and ESR studies of the thermal history of amorphous SiO_2', *J. Non-Cryst. Sol.*, 1985, **71**, pp. 373 – 386.

[72] Kohli, J.T., Condrate, R.A., and Shelby, J.E.: 'Raman and infrared spectra of rare earth aluminosilicate glasses', *Phys. Chem. Glass.*, 1993, **3**4, (3), pp. 81 – 87.

[73] P. Dragic and J. Ballato, "Characterisation of Raman gain spectra in Yb:YAG-derived optical fibres," Electron. Lett. 49, 895–897, 2013.

[74] Shima, K.; Himeno, K.; Sakai, T.; Okude, S.; Wada, A.; Yamauchi, R. A novel temperature-insensitive long-period fiber grating using a boron-doped-germanosilicate-

core fiber. In Proceedings of the Conference on Optical Fiber Communication, Dallas, TX, USA, 16–21 February 1997.

[75] Boling, N.; Glass, A.; Owyoung, A. Empirical Relationships for Predicting Nonlinear Refractive Index Changes in Optical Solids. *IEEE J. Quantum Electron.* **1978**, *QE-14*, 601–608.

[76] Fournier, J.; Snitzer, E. The nonlinear refractive index of glass. *IEEE J. Quantum Electron.* **1974**, *QE-10*, 473–475.

[77] Töpfer, T.; Hein, J.; Philipps, J.; Ehrt, D.; Sauerbrey, E. Tailoring the nonlinear refractive index of fluoride-phosphate glasses for laser applications. *Appl. Phys. B* **2000**, *71*, 203–206.

[78] Agrawal, G.P.; Flytzanis, C. Delocalization and superalternation effects in the nonlinear susceptibilities of one-dimensional systems. *Chem. Phys. Lett.* **1976**, *44*, 366–370.